Marine Chemistry 227 (2020) 103893

Contents lists available at ScienceDirect

Marine Chemistry

journal homepage: www.elsevier.com/locate/marchem

Compositional differences of fluorescent dissolved organic matter in Arctic Ocean spring sea ice and surface waters north of Svalbard

Monika Zabłocka[a,*], Piotr Kowalczuk[a], Justyna Meler[a], Ilka Peeken[b], Katarzyna Dragańska-Deja[a], Aleksandra Winogradow[a]

[a] Institute of Oceanology Polish Academy of Sciences, ul. PowstańcówWarszawy 55, PL-81-712 Sopot, Poland
[b] Alfred-Wegener-Institut Helmholtz-Zentrum für Polar- und Meeresforschung, Polar Biological Oceanography, Bremerhaven, Germany

ARTICLE INFO

Keywords:
Arctic Ocean
Sea ice optical properties
Fluorescent dissolved organic matter (FDOM)
PARAFAC - parallel factor analysis

ABSTRACT

We assessed the qualitative composition of fluorescent dissolved organic matter (FDOM) in Arctic Ocean surface water and in sea ice north of the Svalbard Archipelago (in the Sophia Basin, the Yermak Plateau and the north Spitsbergen shelf) in May and June 2015, during the "TRANSSIZ" expedition (Transitions in the Arctic Seasonal Sea Ice Zone). Samples collected in open lead waters (OW), under-ice waters (UIW) and from the sea ice (ICE) were analyzed by fluorescence spectroscopy and subsequently by multivariate statistical methods using Parallel Factor Analysis (PARAFAC). Statistical analyses of all measured DOM fluorescence excitation and emission matrices (EEMs) enabled four components to be identified and validated. The spectral characteristics of the first component C1 ($\lambda_{Ex}/\lambda_{Em}$ 282(270)/335) corresponded to those of tryptophan. The spectral properties of the other three components corresponded to those of humic-like substances: components two (C2 − $\lambda_{Ex}/\lambda_{Em}$ 315(252)/395) and three (C3 − $\lambda_{Ex}/\lambda_{Em}$ 357(258)/446) corresponded to humic-like substances of marine origin, whereas component four (C4 − $\lambda_{Ex}/\lambda_{Em}$ 261(399)/492) resembled terrestrial humic-like substances. Changes in FDOM composition were recorded in OW, in contrast to UIW and sea ice. In the OW the sum of fluorescence intensities of humic-like components (C2, C3 and C4) was two times higher than the fluorescence intensity of protein-like component (C1). Component C2 exhibited the highest fluorescence intensity. In the UIW and particularly in the sea ice the fluorescence intensity of the protein-like component, I_{C1}, was the highest. The I_{C1} in the sea ice increased toward the sea ice bottom, reaching maximum values at the sea ice-water interface. The calculated spectral indices (SUVA(254) and HIX) and ratios of fluorescence intensities of protein-like to humic-like components, I_p/I_h, suggested that FDOM in water and sea ice was predominantly autochthonous, characterized by low molecular weight organic compounds and low aromatic ring saturation. Enrichment factors D_c, calculated from salinity-normalized values of the optical DOM properties and dissolved organic carbon concentrations, indicated the significant fractionation of FDOM in the sea ice relative to the parent open waters. The humic-like terrestrial component C4 was enriched the least, whereas the protein-like component C1 was enriched the most. A statistically significant ($p < 0.0001$) and relatively strong ($R = 63$) correlation between I_{C1} and the total chlorophyll *a* concentration *Tchla* was found in the sea ice, which suggests that sympagic algal communities were producers of the protein-like FDOM fraction.

1. Introduction

Sea ice differs significantly from other constituents of Earth's cryosphere that originate from freshwater or snow (lake ice, glaciers). The difference is due to sea salt ions, which impact on the formation of ice, its crystalline structure, and its physical and chemical properties (Thomas, 2017 and references therein). Sea ice forms a boundary layer in polar and subpolar marine basins. This insulating layer reduces the heat, mass and momentum exchange between the ocean and atmosphere (McPhee, 2017), alters the surface albedo and reduces radiative energy transfer to the underlying water, which affects the heating rate and primary production by sympagic algae communities and under-ice phytoplankton (Arrigo, 2017). Sea ice, especially in the Arctic Ocean and Antarctica, is a key factor regulating global climatic processes through the so-called sea ice albedo feedback. The sea ice albedo changes seasonally and spatially, and is strongly dependent on sea ice surface properties, reaching a maximum of 0.85 in early spring for snow-covered ice and a minimum in late summer (0.2) for melt pond-covered ice (Perovich, 2017; Perovich et al., 1993; Taskjelle et al., 2016).

* Corresponding author.
E-mail address: monika_z@iopan.pl (M. Zabłocka).

https://doi.org/10.1016/j.marchem.2020.103893
Received 24 March 2020; Received in revised form 7 September 2020; Accepted 16 September 2020
Available online 07 October 2020

With increasing fragmentation of the sea ice cover and the appearance of cracks and leads, the sea ice albedo falls to < 0.2. The rate of solar energy being transmitted through the sea ice depends not only on its thickness, surface properties and fragmentation, but also on the inherent optical properties of the sea ice, i.e., its scattering and absorption coefficients (Perovich, 2017; Taskjelle et al., 2017; Katlein et al., 2019).

The spectral properties and magnitudes of the absorption and scattering coefficients of bulk sea ice depend not only on its crystal structure, the presence of brine channels and impurities such as gas bubbles and particles, but also on the concentration, composition and vertical distribution of absorbing and scattering constituents (Grenfell and Perovich, 1981; Perovich and Govoni, 1991). The absorption and scattering coefficients vary seasonally in magnitude as a result of temporal changes in concentrations of optically significant sea ice constituents contributing to the bulk inherent optical properties and their spectral transformations (Light et al., 2015; Katlein et al., 2019). Assuming that gas bubbles and inorganic sea salt ions do not significantly absorb light at wavelengths greater than 350 nm (Woźniak and Dera, 2007), the main contributors to the sea ice absorption, as in oceanic waters, are ice crystals (water), dissolved and particulate organic matter, particulate mineral matter contained in the ice and brine, and algae growing in the sea ice itself.

Chromophoric dissolved organic matter (CDOM – the optically active fraction of dissolved organic matter DOM) is one of the most optically significant sea water constituents, strongly absorbing light in the UV and visible wavelength ranges. Its absorption spectrum decreases exponentially with increasing wavelengths (Jerlov, 1976). Part of CDOM, known as fluorescent dissolved organic matter (FDOM), has the inherent ability to emit a fraction of the absorbed energy as fluorescence. This property has been known since the late 1930s (Kalle, 1938) and has been used to estimate CDOM in a range of natural waters (Vodacek et al., 1997; Ferrari and Dowell, 1998; Ferrari, 2000). With Excitation Emission Matrix (EEM), a fluorescence spectroscopy technique utilizing emission spectra measurements at a series of successively increasing excitation wavelengths, local fluorescence intensity maxima occurring within characteristic excitation and emission ranges can be assigned to broad classes of dissolved organic compounds constituting DOM (Coble, 1996). Parallel Factor Analysis is a multivariate statistical method which application to DOM biogeochemistry has enabled objective interpretation of EEM spectra and discrimination of different classes of fluorophores based on their excitation/emission maxima (Stedmon et al., 2003). This approach has been used to interpret the multidimensional nature of EEM data sets, and also to study FDOM variability in coastal areas (Stedmon and Markager, 2005a; Kowalczuk et al., 2009), open oceans (Jørgensen et al., 2011; Kowalczuk et al., 2013; Catalá et al., 2016) and in the Arctic Ocean (Dainard and Guéguen, 2013; Guéguen et al., 2014, 2015; Gonçalves-Araujo et al., 2015, 2016). It has improved our understanding of DOM production and degradation in the marine environment (Stedmon and Markager, 2005b), as well as enabling water masses of different origin to be tracked (Gonçalves-Araujo et al., 2016).

The properties of CDOM and FDOM in the sea ice have been studied during different phases of its formation, persistence and melting, mostly in the Baltic Sea, (Ehn et al., 2004; Stedmon et al., 2007; Uusikivi et al., 2010; Müller et al., 2011), the Chukchi Sea and Canadian Arctic (Xie et al., 2014; Logvinova et al., 2016; Hill and Zimmerman, 2016), Antarctica (Norman et al., 2011), and in indoor experiments under controlled conditions (Müller et al., 2011, 2013). It has been found that a high proportion of DOM/CDOM is rejected from the ice crystal structure with the brine during ice formation, although a small fraction of it remains incorporated within the ice and persists in brine channels (Müller et al., 2013; Hill and Zimmerman, 2016). During the ice formation, DOM remaining in the ice undergoes significant fractionation. The humic-like fraction is the most susceptible to rejection from the sea ice along with the brine during freezing, whereas the protein-like DOM fraction is the least susceptible to this process, which shifts the molecular composition of DOM toward a higher proportion of low molecular weight (LMW) compounds (Müller et al., 2013; Granskog et al., 2015b; Retelletti-Brogi et al., 2018). The intensive growth of sympagic algae in spring and the associated production of organic matter further contribute to the accumulation of LMW organic matter in the sea ice (Stedmon et al., 2007). Significant in situ production of DOM/CDOM by sympagic autotrophic organisms inhabiting land-fast sea ice in the Canadian Archipelago was documented by Xie et al. (2014). The composition of DOM/CDOM and its associated optical properties may be further modified by photochemical and microbial transformations (Stedmon et al., 2007).

The optical properties of the sea ice north of Svalbard were described by Kowalczuk et al. (2017) and Kauko et al. (2017), who reported much lower CDOM absorption in the sea ice and under-ice waters than in the Western Arctic Ocean and over the Siberian Shelf. The properties, distribution and cycling of FDOM in the sea ice in the Atlantic sector of the Arctic Ocean have not been studied to date. The main aim of this research was to: *i*) assess the DOM composition in the sea ice and underlying waters in early spring on the basis of fluorescence spectroscopy, multivariate statistical models (PARAFAC) and calculated spectral indices; *ii*) analyze the distribution of identified FDOM components and spectral indices in the vertical profiles within the sea ice and under-ice water; *iii*) relate measured DOM optical signatures to concentrations of dissolved organic carbon and chlorophyll *a*.

2. Materials and methods

2.1. The study area

Sea ice and water samples were collected north of Svalbard, in the northern extension of its shelf, the Sophia Basin and the Yermak Plateau (Table 1, Fig. 1). This is an important region, where warm Atlantic Water (AW) carrying heat and salt into the Arctic Ocean interfaces Polar Water (PW) (Aagaard et al., 1987). More than 30% of the total AW that flows through the Fram Strait into the Arctic is carried by the West Spitsbergen Current (WSC) (Beszczynska-Möller et al., 2012), a northward flowing extension of the Norwegian Atlantic Current (NAC). At about 80°N, WSC splits into two branches: the Svalbard Branch (SB) and the Yermak Plateau Branch (YPB). The SB follows the continental shelf while the YPB moves northwestward until about 81°N, where warm WSC waters meet ice transported by the Transpolar Drift from the eastern Arctic seas north of Svalbard. This region, known as Whalers Bay, has become ice-free as a result of intense ice melting (Onarheim et al., 2014). Apart from melting the ice from below (Polyakov et al., 2017), the Atlantic waters also inhibit ice growth during winter. In consequence, during the last few decades, the ice edge as a whole has been retreating farther north of Svalbard. The largest contraction of the ice north of Svalbard occurs during winter, which is in contrast to the changes observed in central parts of the Arctic Ocean (Onarheim et al., 2014). Increasing volumes of warm AW intrusions have caused the ice pack carried by the Transpolar Drift to move into thinner and younger sea ice during recent decades (Hansen et al., 2013; Renner et al., 2014).

2.2. Sample collection and processing

Water and sea ice samples were collected during the “TRANSSIZ” expedition (Transitions in the Arctic Seasonal Sea Ice Zone) on board the icebreaker FS Polarstern in May and June 2015 (cruise code PS92 - ARK XXIX/1) (Peeken, 2016). The field work was conducted in the sea ice covered waters. All together we collected 84 OW samples, 16 UIW samples and 58 ICE samples. Detailed information on the water and sea ice-water stations visited during the cruise is given in Table 1.

2.2.1. Sea ice sampling

Sea ice sampling involved the collection of sea ice for determining biological, physical and chemical parameters with Kovacs Mark II or Mark V coring systems (Kovacs Enterprise, Roseburg, USA). Three separate sea ice cores were collected in order to obtain the parameters discussed in this article: one physical core, which was used to measure temperature and salinity, CDOM absorption and dissolved organic carbon concentration; and

Table 1
Dates, positions, number of samples (N) collected in OW, UIW and ICE and parameters measured during the TRANSSIZ expedition.

Cruise/Station	Date	Position		N			Ice thickness [m]	Snow thickness [m]
		Latitude N [deg]	Longitude E [deg]	OW	UIW	ICE		
				Sea ice-water stations				
PS92/19	2015.05.28	81.1734	19.136	7	2	11	0.93	0.24
PS92/27	2015.05.31	81.3858	17.589	6	2	8	1	0.27
PS92/31	2015.06.03	81.6209	19.4342	5	2	7	1.19	0.36
PS92/32	2015.06.06–07	81.234	19.4292	6	2	6	1.11	0.26
PS92/39	2015.06.11	81.9222	13.4867	4	2	7	1.26	0.18
PS92/43	2015.06.15	82.2108	7.5933	6	2	6	1.05	0.2
PS92/46	2015.06.17–18	81.8907	9.7282	6	2	7	1.3	0.1
PS92/47	2015.06.19–20	81.3482	13.6121	6	2	6	1.01	0.14
				Water stations				
PS92/21	2015.05.30	81.0725	18.926	6	–	–	–	–
PS92/24	2015.05.30	81.2767	18.6726	6	–	–	–	–
PS92/29	2015.05.31	81.5802	19.8335	6	–	–	–	–
PS92/36	2015.06.09	81.3403	16.7187	6	–	–	–	–
PS92/52	2015.06.22	81.1178	9.7443	7	–	–	–	–
PS92/56	2015.06.23	81.0163	8.271	7	–	–	–	–
All data				84	16	58		

Note: Sampling of the physical, optical and bio-optical parameters during the TRANSSIZ cruise included temperature, salinity, $a_{CDOM}(\lambda)$, FDOM, chlorophyll *a* concentration, *Tchla,* and was conducted in: the open leads water column (OW), under sea ice water column (UIW) and sea ice (ICE).

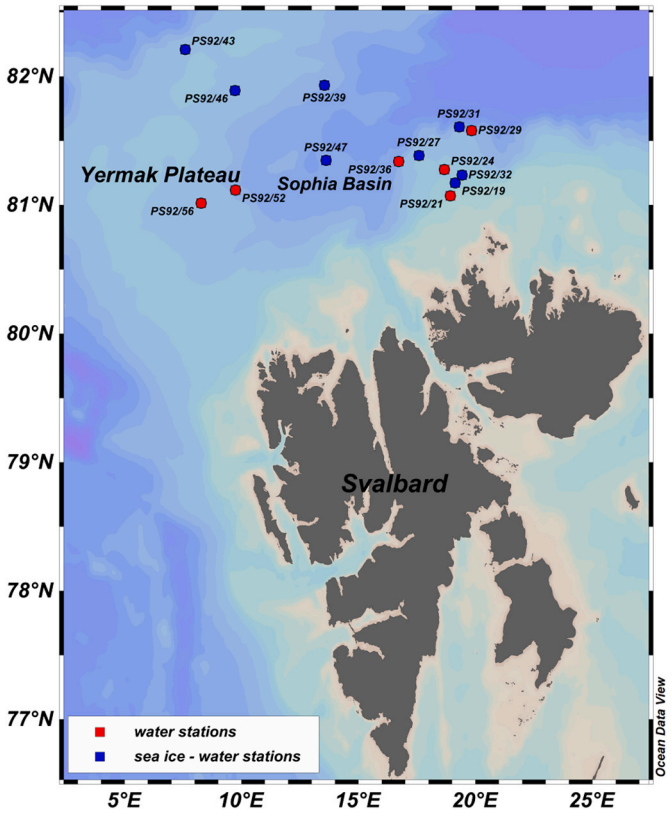

Fig. 1. Location of the sampling stations during the TRANSSIZ (PS92) expedition.

another two for determining biological variables, including the chlorophyll *a* concentration (from pigment analysis). The temperature in the physical core was measured with a Testo 720 probe (Testo Electronics, Lenzkirch, Germany) every 5 cm. Thereafter, the core was cut into 10 cm sections, placed in acid-cleaned high-density polyethylene (HDPE) cups and immediately stored in a cooling box prior to transportation to the ship. Because of the high concentration of algae at the bottom of the ice core, the length of the last (bottom) section was 5 cm. One of the "biological" cores was also cut into 10 cm pieces, except for the last 5 cm, which was pooled with the last 5 cm section from the second "biological" core (to obtain a sufficient volume of melt water). All the "biological" core sections were melted in sea water previously passed through a 0.2 µm filter in order to minimize the osmotic stress on protists during the melting process (Miller et al., 2015). Sections from the cores were stored in a fridge at 4 °C and kept in the dark until melted. In the physical core, salinity was measured with a Salinometer WTW Cond 3110 (Wissenschaftlich-Technische Werkstätten, Weilheim, Germany) and the remaining water was used for all the variables except chlorophyll *a*. To obtain the volume of the melt water required for measuring the biological parameters listed above, water from two adjacent sections, starting from the sea ice surface, was pooled. The last 5 cm sections were not pooled with the overlying ice sections.

2.2.2. Water sampling

Water column samples from the open lead waters (OW) were collected with a rosette water sampler system (Sea-Bird Electronics Inc.), deployed by the side of the ship and equipped with 24 12-l Niskin bottles. The water column was sampled at the depths – 5, 10, 20, 30, 75, 100 m and just above the sea bed. Additionally, at every ice station, the under-ice water (UIW) was collected using a Kemmerer-type bottle deployed manually through the drill holes from which the sea ice cores were extracted. UIW was sampled directly from beneath the sea ice cover (0 m) and from the chlorophyll *a* maximum depth, determined with a CYCLOPS-7 submersible fluorometer (Turner Designs, Sunnyvale, CA, USA), attached to a Sea and Sun CTD75M probe (Sea and Sun Technology, Trappenkamp, Germany). The CTD75M probe was lowered manually through an sea ice hole. The depth of the Kemmerer bottle sampling was measured with a metered rope.

2.2.3. Sample processing

Water column samples collected for CDOM, FDOM and DOC concentration were filtered gravitationally through an Opticap XL4 Durapore flow-through filter cartridge of nominal pore size 0.2 µm, attached directly to the Niskin bottle tap. To prevent sample contamination, the cartridge filter and tubing were stored in 10% aq. HCl and rinsed with ultrapure MilliQ and sample water before sample collection. Sea ice melt water (ICE) samples and UIW samples for determining CDOM, FDOM and DOC were filtered twice: once through Whatman glass-fiber filters (GF/F, nominal pore size 0.7 µm) and then through acid-washed Sartorius 0.2 µm pore size cellulose membrane

filters. The 0.2 µm sterile syringe filter (VWR cellulose acetate membrane) attached to a 150 mL acid-washed plastic syringe were used to filter sea ice melt water from the last 5 cm sea ice cores sections to collect CDOM, FDOM and DOC samples. The samples for determining DOC were acidified with 150 µL 0.1 M HCl. All samples were filtered into pre-combusted amber glass vials and stored at 4 °C in the dark, which preserves DOM optical properties for several weeks (Stedmon and Markager, 2001).

Water column, UIW and melted sea ice samples collected for HPLC (high performance liquid chromatography) pigment analysis were passed through Whatman 25 mm GF/F filters. The filter pads with material retained on them were immediately immersed in liquid nitrogen and thereafter stored at −80 °C prior to analysis.

2.2.4. CDOM absorption measurements

During the TRANSSIZ expedition, CDOM absorption was measured on board the FS Polarstern immediately after filtration using a double-beam Perkin-Elmer Lambda-35 spectrophotometer in the spectral range 240–700 nm. The measurements were done in a 10-cm quartz cell, with fresh ultrapure water as reference. The CDOM absorption coefficient $a_{CDOM}(\lambda)$ was calculated using the equation:

$$a_{CDOM}(\lambda) = 2.303\, A(\lambda)/l \quad (1)$$

where $A(\lambda)$ is the absorbance, l is the optical path length in meters and the factor 2.303 is the natural logarithm of 10.

The CDOM absorption spectrum slope coefficient $S_{350\text{-}600}$ was calculated in the 350–600 nm spectral range using a nonlinear least squares fitting method with the Trust-Region algorithm implemented in Matlab R2013 (Stedmon et al., 2000; Kowalczuk et al., 2006). The method uses the equation:

$$a_{CDOM}(\lambda) = a_{CDOM}(\lambda_0)e^{-S(\lambda_0-\lambda)} + K \quad (2)$$

where λ_0 is 350 nm, and K is a background constant of the baseline shift resulting from the residual scattering by fine size particle fractions, micro-air bubbles or colloidal material present in the sample, refractive index differences between the sample and the reference, or attenuation not due to CDOM.

2.2.5. DOM fluorescence measurements and the PARAFAC model

Fluorescence Excitation Emission Matrix spectra (EEM) of the DOM samples collected during TRANSSIZ were measured in the laboratory at the Institute of Oceanology Polish Academy of Sciences (IOPAN – Sopot, Poland) with a HORIBA Aqualog spectrofluorometer in a 1 cm quartz cuvette. The excitation spectral range was set at 240–600 nm with a 3 nm increment. The emission spectral range was recorded between 246.65 and 829.44 nm with a 2.33 nm increment. The emission signal integration time was 8 s. All the EEM spectra acquired were spectrally corrected with a set of instrument-dependent correction coefficients internally implemented within the spectrofluorometer.

The excitation and emission matrix spectra were processed using the drEEM toolbox implemented in the Matlab 2013R computing environment, in accordance with the procedures described by Stedmon and Bro (2008) and Murphy et al. (2010, 2013). The spectrally corrected samples were calibrated and normalized against the Raman scatter emission peak of the MilliQ water sample, run on the same day, excited at a wavelength of 351 nm and integrated in the spectral range 378–424 nm. The resulting EEM spectra were scaled in Raman units (R.U., [nm^{-1}]). Samples were corrected for inner filter effects using the CDOM absorption spectra of the corresponding water samples (section 2.2.4). The blank MilliQ water sample, corrected and calibrated in the same way as the regular samples, was subtracted from each measured EEM to remove the Raman scattering signal. The PARAFC model was applied to the data array, the dimensions of which consisted of 168 samples × 121 excitations × 153 emissions. The PARAFAC model was run with a non-negativity constraint on the assumption that signals from a complex mixture of DOM compounds can be separated and that the components differ from each other spectrally. The PARAFC model results were validated by split-half validation (Harshman, 1984) applied to independent sub datasets (S4C6T3 – Splits, Combinations, Tests). A four component model was successfully validated.

2.2.6. HPLC measurements

The HPLC chlorophyll samples from TRANSSIZ ice melt water were measured using a Waters 1525 binary pump equipped with an auto sampler (OPTIMAS™), a Waters photodiode array and fluorescence detectors (2996, 2475, respectively), and EMPOWER software. To each filter sample 50 µL of canthaxanthin (internal standard) and 1.5 mL of acetone were added and then homogenized for 20 s in a Precellys® tissue homogenizer. After centrifugation, the supernatant liquids were passed through 0.2 µm PTFE filters (Rotilabo). Aliquots of 100 µL were transferred into the auto sampler (4 °C), premixed with 1 M ammonium acetate solution (1:1) and injected into the HPLC-system. Pigments were analyzed by reverse-phase HPLC using a VARIAN Microsorb-MV3 C8 column (4.6 × 100 mm) and HPLC-grade solvents (Merck). Solvent A consisted of 70% methanol and 30% 1 M ammonium acetate, and solvent B consisted of 100% methanol. The gradient was modified after Barlow et al. (1997). Eluting pigments were detected by absorbance (440 nm) and fluorescence (Ex: 410 nm, Em: > 600 nm), and chlorophyll *a* was identified by comparing their retention times with those of pure standards. Additional confirmation was obtained by comparing the spectra with the on-line diode array absorbance spectra between 390 and 750 nm stored in the library from the pure standards. The total chlorophyll concentration, *Tchla*, was calculated as the sum of chlorophyll *a* and its allomers and epimers concentrations measured with HPLC methods.

2.2.7. DOC concentrations

Concentrations of Dissolved Organic Carbon (DOC) were measured in a HiPerTOC analyzer (Thermo Electron Corp., the Netherlands). The method used was based on UV/persulphate oxidation and NDIR (Non Dispersive Infra-Red) detection of evolving CO_2 (Sharp, 2002). To remove dissolved CO_2, each sample was purged with synthetic air. The precision of the measurement was determined from a triplicate analysis of each sample. Quality control consisted of the regular analysis of blanks as well as accuracy checks based on comparisons with the reference material supplied by the Dennis Hansell Laboratory (University of Miami). The methodology ensured satisfactory accuracy (average recovery 93.1% of the certified CRM value; $n = 5$) and precision characterized by a relative standard deviation (RSD) of 2.5%.

2.2.8. Spectral indices

Following spectral indices, widely used in aquatic DOM biogeochemistry, based on CDOM absorption and DOM fluorescence spectra were calculated to quantify structural and compositional changes in DOM: *i*) humification index – HIX, which is related to C/H ratio in DOM molecular structure, was calculated from the original EEMs, according to Zsolnay et al. (1999) as the ratio of the emission spectrum (excited at 255 nm) integral over the spectral range 434–480 nm, $\sum_{434}^{480} I_{(ex.255)}$, to the emission spectrum integral over the spectral range 300–346 nm (excited at the same wavelengths), $\sum_{300}^{346} I_{(ex.250)}$:

$$HIX = \frac{H}{L} = \frac{\sum_{480}^{434} I_{(ex.255)}}{\sum_{345}^{300} I_{(ex.255)}} \quad (3)$$

ii) I_p/I_h calculated as the ratio of the fluorescence intensity of identified protein-like components to the sum of fluorescence intensities of identified humic-like components:

$$I_p/I_h = \frac{I_{C1}}{I_{C2} + I_{C3} + I_{C4}} \quad (4)$$

where I_{Cn} is the intensity of the respective component from one through

Table 2
Ranges of variability, median and 1st and 3rd quartiles of the physical properties of ice and oceanic water and the optical properties of CDOM, in different environments. N – number of measurements.

Samples description	Temperature [°C]	Salinity	*Tchla* [mg m^{-3}]	$a_{CDOM}(350)$ [m^{-1}]	Spectral slope $S_{350\text{-}600}$[nm^{-1}]
			Open leads water column		
Surface layer (0-35 m)	−1.83 to −1.19	33.78–34.43	0.24–10.19	0.100–0.231	0.010–0.017
Median	−1.71	34.14	1.92	0.149	0.014
Q_1;Q_3	−1.77; −1.59	34.04; 34.29	0.36; 4.03	0.140; 0.163	0.013; 0.015
N	39	39	20	38	38
Below chlorophyll max. Layer (35-200 m)	−1.83– 2.56	34.13–34.97	0.03–3.09	0.090–0.195	0.012–0.018
Median	−0.11	34.64	0.47	0.137	0.014
Q_1;Q_3	−1.02; 2 01	34.38; 34.89	0.16; 1.74	0.132; 0.150	0,014; 0.015
N	35	35	20	35	35
			Under sea ice water column		
Surface (0 m)	−2.00 to −1.05	26.04–34.06	0.48–4.84	0.152–0.233	0.013–0.018
Median	−1.51	27.95	1.57	0.184	0.016
Q_1;Q_3	−1.73; −1.27	27.46; 31.58	0.59; 2.65	0.161; 0.214	0.016; 0.017
N	8	8	8	8	8
Chlorophyll max. depth (3-25 m)	−1.84 to −1.63	33.75–34.47	0.29–7.46	0.128–0.227	0.011–0.017
Median	−1.73	34.16	1.81	0.184	0.016
Q_1;Q_3	−1.81; −1.67	34.10; 34.35	0.60; 3.24	0.153; 0.202	0.015; 0.017
N	7	7	8	8	8
			sea ice		
Surface layer (0-33.3%), N = 19	−3.33 to −0.20	0.05–10.6	0.11–0.82	0.047–0.663	0.013–0.031
Median	−1.90	5.60	0.36	0.102	0.020
Q_1;Q_3	−2.58; −1.00	3.47; 7.85	0.28; 0.58	0.076; 0.159	0.020; 0.023
Middle layer (33.3-66.6%), N = 17	−3.33 to −0.58	0.25–7.1	0.15–1.91	0.036–0.197	0.012–0.024
Median	−1.98	4.65	0.63	0.061	0.018
Q_1;Q_3	−2.48; −1.36	0.75; 5.15	0.44; 0.81	0.053; 0.119	0.016; 0.021
Bottom layer (66.6-100%), N = 21	−2.87 to −0.98	1.65–3.2	0.39–8.90	0.049–0.465	0.011–0.036
Median	−1.60	5.10	2.55	0.156	0.020
Q_1;Q_3	−2.05; −1.30	4.60; 5.80	0.65; 5.03	0.086; 0.252	0.015; 0.024

four (C1 to C4) identified by the PARAFAC model. The spectral characteristics and origins of these components are explained in the Results section and listed in Table 3.

iii) the carbon specific absorption coefficient at 254 nm – SUVA(254). This describes the relative aromaticity of DOM and is linearly correlated with the percentage aromatic ring saturation of the DOM mixture (Weishaar et al., 2003); low values refer to DOM with a dominant aliphatic structure and low aromatic ring saturation. This index was calculated as follows:

$$SUVA(254) = \frac{a_{CDOM}(254)}{DOC} \quad (5)$$

where $a_{CDOM}(254)$ is the CDOM absorption coefficient at 254 nm and DOC is the dissolved organic carbon concentration.

2.2.9. Enrichment factors

During sea ice formation, DOM, together with inorganic dissolved constituents of water, is gradually rejected from the crystalline ice structure. These non-linear processes, leading to the enrichment of CDOM and FDOM in the ice relative to salinity, can be quantified using the formula given by Müller et al. (2011):

$$D_c = \frac{\left(\frac{C}{S}\right)_i - \left(\frac{C}{S}\right)_w}{\left(\frac{C}{S}\right)_w} \quad (6)$$

where C denotes the concentration/quantity of given parameter, S denotes the salinity and subscripts i and w refer to ICE and OW, respectively. The median values of enrichment factors D_c were calculated for three sea ice sections (surface, middle and bottom) and also for the last 5 cm of the sea ice (Table 6).

We calculated the enrichment factors D_c for the following parameters: CDOM absorption coefficient at 350 nm ($a_{CDOM}(350)$), the fluorescence intensities of each identified fluorophore (I_{C1} through I_{C4}), the total fluorescence intensity (I_{tot}) and the dissolved organic carbon concentration (DOC), normalizing the respective values with respect to the relevant salinity (C/S). As we did not know the initial conditions during ice formation, we assumed after Kowalczuk et al. (2017) that salinity and the optical properties of CDOM and FDOM, i.e. $a_{CDOM}(350)$, I_{Cn}, and I_{tot} and DOC, were close to those observed in the surface layer of OW (Tables 2, 4 and 5).

2.2.10. Statistical analysis

The statistical Shapiro-Wilk test has been performed in the initial phase of the data analysis to check whenever analyzed parameter conform the normal distribution. Most of considered parameters failed the conformity with normal distribution, therefore the percentiles and median values were chose to reflect observed distribution of parameters values. The Mann-Whitney U test has been applied to check the significance in reported differences in median values.

3. Results

3.1. Spring hydrological conditions and bio-optical properties of Arctic Ocean waters and sea ice north of Svalbard

The hydrological and bio-optical conditions of OW and UIW have been described in detail by Kowalczuk et al. (2017), Kauko et al. (2017) and Pavlov et al. (2017), who found statistically significant differences

in the bio-optical properties of Arctic Ocean waters in open leads and under sea ice. To be consistent with Kowalczuk et al. (2017), we have applied the same criteria, creating a data subsets according to the vertical distribution of optical properties in water and sea ice. We now summarize selected published results so as to provide a wider context for the current study.

The surface water temperature was near freezing point. That remnant of the cold mixed layer formed in winter reached ca 80 m depth and was present at most stations sampled (Kowalczuk et al., 2017) except PS92/27 and PS92/31 and to a lesser extent PS92/19 and PS92/32. These stations, located near the north Svalbard shelf, lay on the path of inflowing Atlantic waters (AW). Advection of warm AW gave rise to significant thermo- and haloclines, and the depth of the winter mixed layer was reduced to ca 20 m. Salinities at all ice stations were higher than 34 (Meyer et al., 2017), indicating the strong influence of Atlantic waters. Salinity measurements beneath the sea ice revealed a strong gradient in a thin layer below the sea ice. This feature was observed at all the sea ice stations except PS92/43 and PS92/46 and was an indicator of the initial phase of sea ice melting (Kowalczuk et al., 2017). The chlorophyll *a* concentration measured in the south-eastern part of the sampled area (four ice-water stations: PS92/19, PS92/27, PS92/32, PS92/47 and three water stations: PS92/21, PS92/24, PS92/36) was high, up to 7.4 mg m^{-3}, indicating growth of the under-ice phytoplankton bloom (Pavlov et al., 2017). CDOM absorption was low and within the range of values reported for this area (Pavlov et al., 2015; Gonçalves-Araujo et al., 2018). The ranges of $a_{CDOM}(350)$ were 0.090–0.231 m^{-1} in OW, 0.128–0.233 m^{-1} in UIW and 0.036–0.663 m^{-1} in the sea ice (Table 2). The ranges of $S_{350\text{-}600}$ were 0.010–0.018 nm^{-1} in OW, 0.011–0.018 nm^{-1} in UIW and 0.011–0.036 nm^{-1} in the sea ice (Table 2). Median values of $a_{CDOM}(350)$ in UIW were higher than CDOM absorption in OW and sea ice (Table 2).

The sea ice varied in thickness from 0.93 to 1.3 m (Table 1). Owing to the considerable variability in the sea ice thickness, the sea ice depth was presented as the percentage core thickness relative to the top of each core, and all results related to the vertical distribution of the sea ice's physical properties. DOM optical properties were thus expressed as a function of relative thickness. The salinity of sea ice was low – between 0.05 and 10.6 – and its temperature ranged between - 3.33 and - 0.20 °C, which was characteristic of a mixture of first-year and second-year ice (Granskog et al., 2017). The median of sea ice salinity decreased toward the bottom of the ice, while the lowest median temperature was measured in the middle of sea ice section, with elevated values in the surface and bottom sea ice (Table 2 and Fig. 2).

Median $a_{CDOM}(350)$ values in the sea ice were similar to those reported in OW but lower than in UIW (Table 2). The vertical distributions of the $a_{CDOM}(350)$ and spectral slope coefficient $S_{350\text{-}600}$ values were elevated at the surface and bottom of the sea ice and minimum median values in the middle of the sea ice, (Fig. 2).

Median *Tchla* was lower in the sea ice than in OW and UIW (Table 2). However, chlorophyll *a* was concentrated in the bottom section of the sea ice (66–100% relative ice depth), with the highest value (8.90 mg m^{-3}) in the last 5 cm of the sea ice (on station PS92/31). The *Tchla* distribution was typically L-shaped (see e.g., Hill and Zimmerman (2016), Kowalczuk et al. (2017), Kauko et al. (2017)). *Tchla* increased systematically during the four weeks of observation (Kowalczuk et al., 2017; Kauko et al., 2017; Pavlov et al., 2017), reflecting the increasing light transmission through the sea ice algae biomass (Massicotte et al., 2019).

The DOC levels reported in this study lay within the variability ranges from 33.83 µmol dm^{-3} in the middle layer of the sea ice to 139.42 µmol dm^{-3} in the OW surface. The range of variability was the smallest in the UIW (70.64–124.83 µmol dm^{-3}) and the biggest in the sea ice (139.42–126.17 µmol dm^{-3}). Median DOC values were the highest in the UIW reaching 88.25 µmol dm^{-3} in water just below the sea ice cover and the smallest in the sea ice (48.25 µmol dm^{-3}, in the bottom layer of the ICE). Median DOC values in the OW were between those observed in UIW and ICE (Table 5).

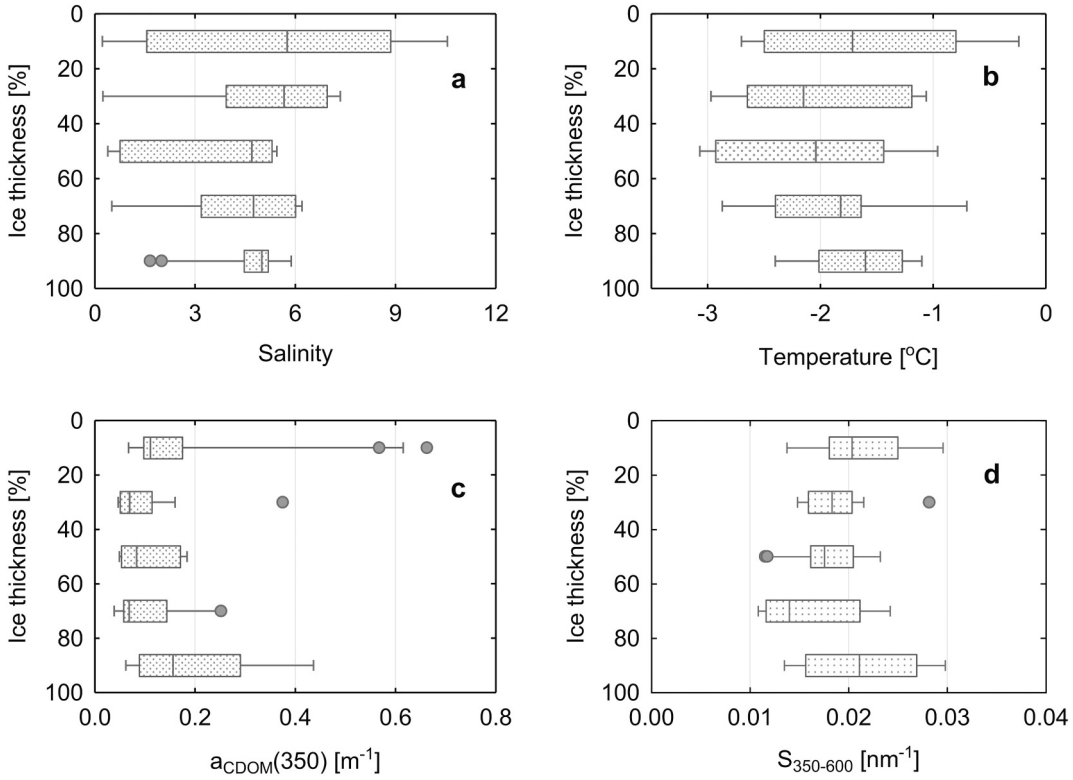

Fig. 2. Vertical profiles of: a) salinity, b) temperature, c) $a_{CDOM}(350)$ and d) $S_{350\text{-}600}$ in the sea ice sections. The sea ice thickness is given as a percentage were 0% is the top of the sea ice and 100% is the bottom of the sea ice (interacting with sea water). Median values are indicated by solid lines, 10th and 90th percentiles by whiskers and 25th and 75th percentiles boxes. The outliers are presented by dots.

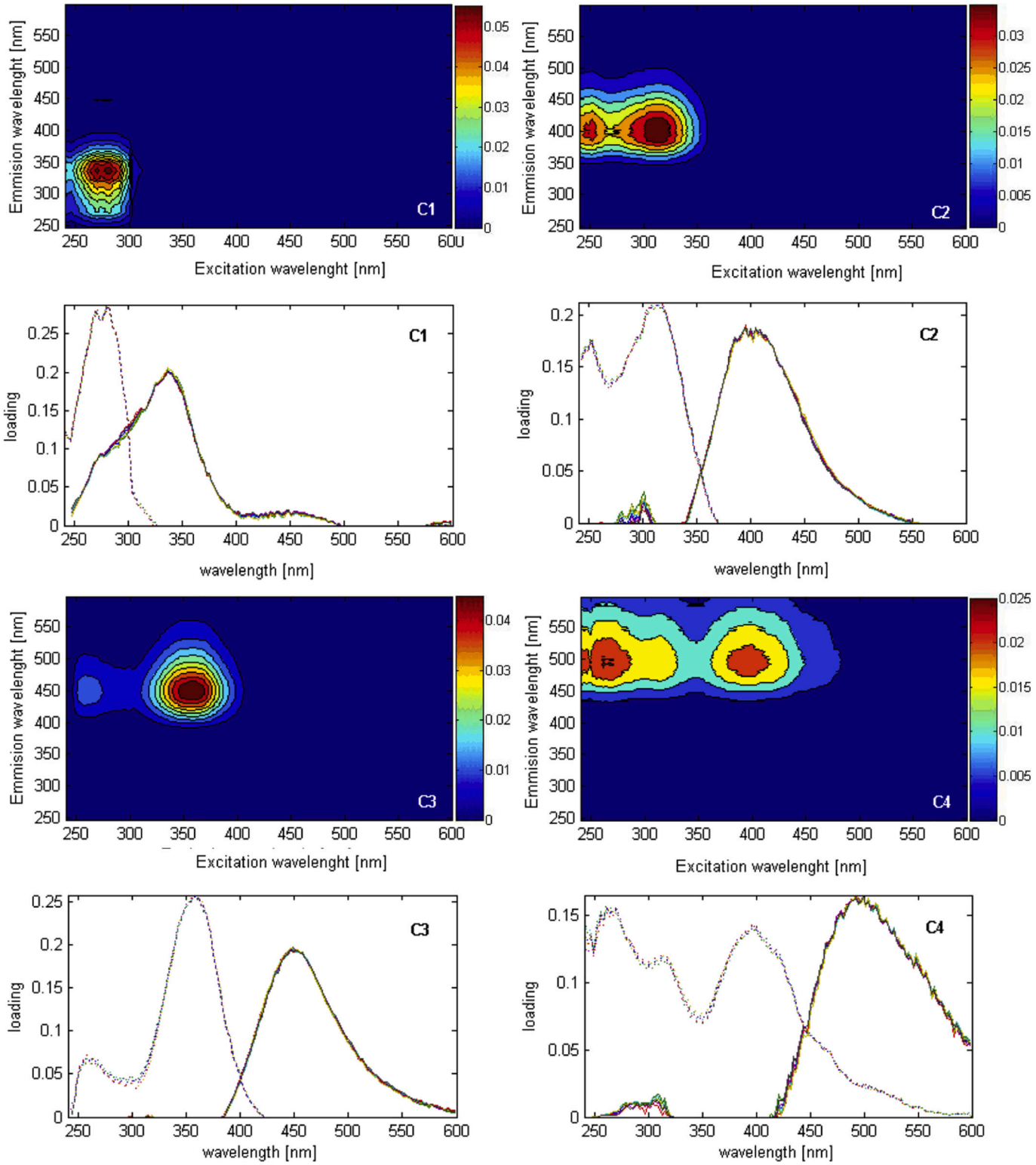

Fig. 3. The PARAFAC output showing the fluorescence signatures of the four components identified in the whole data set. The colorbars indicate the fluorescence intensities in R.U. The line plots ilustrate the spectral shapes of the excitation (dashed lines) and emission (solid lines) of the components.

3.2. PARAFAC model output

The contour plots and the excitation and emission spectra loadings of the identified components together with the split-half validation results are presented in Fig. 3. The excitation and emission characteristics of the modeled components are listed in Table 3. The PAPRAFAC model identified one protein-like component (C1) and three humic-like components (C2 through C4) in our data set. The excitation/emission characteristics of component one (C1) ($\lambda_{Ex}/\lambda_{Em}$ 282(270)/335) resemble the spectral characteristics of tryptophan. Those of component two (C2) ($\lambda_{Ex}/\lambda_{Em}$ 315(252)/395) resemble the peak M described by Coble (1996), so that C2 is considered to be a precursor of organic matter of marine origin. The second humic-like component C3 ($\lambda_{Ex}/\lambda_{Em}$ 357(258)/446) has spectral characteristics similar to those of the terrestrial humic-like material described by

Table 3
Excitation and emission spectral characterization of four components identified by PARAFAC in analyzed data set along with their comparisson with Coble (1996) and other authors (OpenFluor[a] database).

Component no.	Excitation maximum λ_{Ex} [nm]	Emission maximum λ_{Em} [nm]	Coble (1996) * Stedmon et al. (2003)	Probable source	Model
				Amino acids, free or bound in proteins	
1	282(270)	335	T peak 275/340	Component C6:275/328	Omdrev[b]
				Component C3: 280(250)/342	Okhotsk_sea_ice[c]
				Component C5: 270/332	SAB6_2001_2005[d]
				Component C3: 275/340	Antarctic[e]
				Humic-like substances	
2	315(252)	395	M peak 312/380–420	Component C2:250(310)/400	Omdrev[a]
				Component C1: 250(295)/385	Okhotsk_sea_ice [b]
				Component C3: 250(310)/400	SAB6_2001_2005[c]
				Component C6: 325/396	Antarctic[d]
3	357(258)	446	C peak 350/420–480	Component C2: 260(340)442	Okhotsk_sea_ice [b]
				Component C3: 345/448	CS_Flocc[f]
4	261(399)	492	A + *D peak A peak 260/380–460 D peak 390/509	Component C3:280(400)/504	Omdrev[a]
				Component C4: < 300/498	CS_Flocc[5]

[a] Murphy et al., 2014
[b] Kothawala et al., 2014
[c] Granskog et al., 2015b
[d] Kowalczuk et al., 2009
[e] Stedmon et al., 2011b
[f] Søndergaard et al., 2003

Coble (1996) as peak C. We consider the spectral characteristics of the component four (C4) ($\lambda_{Ex}/\lambda_{Em}$ 261(399)/492) to be a mixture of humic-like material of terrestrial origin, described earlier as peak A(Coble, 1996), and soil fulvic acids – peak D (Stedmon et al., 2003). We compared the components identified in this study with those identified in different environments by other scientists and stored in the "OpenFluor" spectral library (Murphy et al., 2014). Table 3 compares the spectral properties of FDOM components identified in this study and matching examples selected from "OpenFluor" data base.

3.3. Distribution of FDOM components in OW, UIW and sea ice

There were differences in FDOM composition in the two water types (OW and UIW) and the sea ice. The bar plots in Fig. 4 illustrate the median

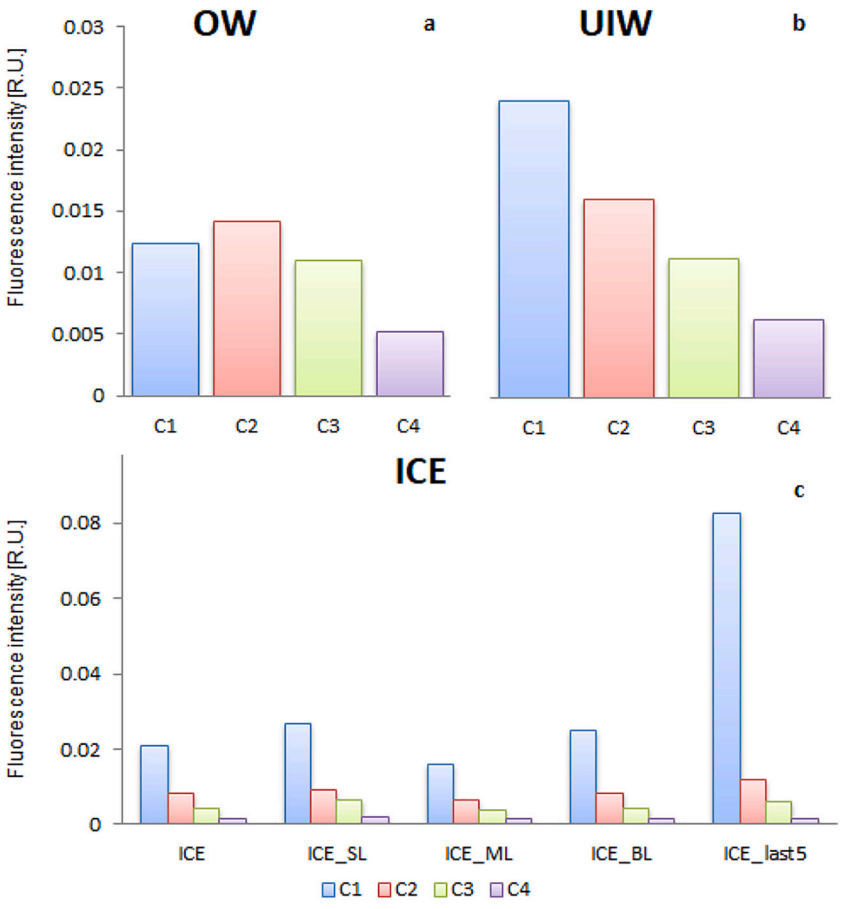

Fig. 4. Distribution of the fluorescence intesites of components C1 through C4 in three distinct environments: a) OW – Open Water, b) UIW – Under Ice Water and c) sea ice – ICE. The sea ice data were additionally split into 4 subsets: surface layer - ICE_SL, middle layer - ICE_ML, bottom layer - ICE_BL, and the last 5 cm in the bottom layer - ICE_last5 (c). The samples from two depth ranges in OW and UIW were pooled together. The bar plots represent the median fluorescence intensities of components C1 through C4.

Table 4
Ranges of variability, median and 1st and 3rd quartiles of fluorescence intensities of four derived components and total fluorescence intensity, in different environments. N – number of measurements.

Samples description	I_{C1} [R.U.]	I_{C2} [R.U.]	I_{C3} [R.U.]	I_{C4} [R.U.]	I_{tot} [R.U.]
Open leads water column					
Surface layer (0-35 m), N = 39	0.005–0.071	0.008–0.026	0.008–0.20	0.002–0.009	0.025–0.115
Median	0.014	0.014	0.01	0.005	0.044
Q_1;Q_3	0.011; 0.016	0.013; 0.015	0.009; 0.015	0.005; 0.006	0.041; 0.050
Below chlorophyll max. Layer (35-200 m), N = 35	0.006–0.035	0.009–0.016	0.008–0.019	0.002–0.006	0.031–0.066
Median	0.012	0.014	0.01	0.005	0.042
Q_1;Q_3	0.010; 0.013	0.013; 0.015	0.010; 0.014	0.005; 0.006	0.039; 0.045
Under sea ice water column					
Surface (0 m), N = 14	0.014–0.005	0.015–0.021	0.009–0.018	0.005–0.008	0.046–0.072
Median	0.024	0.015	0.011	0.006	0.056
Q_1;Q_3	0.019; 0.025	0.015; 0.016	0.010; 0.014	0.006; 0.006	0.055; 0.058
Chlorophyll max. depth (3–25 m), N = 8	0.013–0.060	0.013–0.020	0.010–0.017	0.005–0.008	0.042–0.097
Median	0.024	0.017	0.011	0.006	0.057
Q_1;Q_3	0.018; 0.032	0.015; 0.019	0.010; 0.013	0.006; 0.007	0.051; 0.072
Sea ice					
Surface layer (0 - 33.3 %), N = 19	0.013–0052	0.005–0.019	0.003–0.030	0.001–0.005	0.023–0.105
Median	0.027	0.009	0.007	0.002	0.048
Q_1;Q_3	0.018; 0.031	0.007; 0.011	0.004; 0.026	0.002; 0.003	0.060; 0.069
Middle layer (33.3 - 66.6 %), N = 17	0.010–0.032	0.004–0.012	0.003–0.029	0.001–0.003	0.018–0.064
Median	0.016	0.007	0.004	0.002	0.03
Q_1;Q_3	0.014; 0.021	0.005; 0.008	0.004; 0.011	0.001; 0.002	0.026; 0.037
Bottom layer (66.6 - 100 %), N = 21	0.010–0.246	0.006–0.021	0.003–0.031	0.001–0.004	0.020–0.299
Median	0.025	0.009	0.004	0.002	0.055
Q_1;Q_3	0.016; 0.059	0.007; 0.012	0.003; 0.023	0.001; 0.002	0.028; 0.081

fluorescence intensity of each component in the two water masses. The third data set – sea ice (ICE) – was divided into three main vertical subsets: surface layer, middle layer and bottom layer, with the additional forth layer - last 5 cm layer - subtracted from the bottom layer. The statistical data relating to the total fluorescence intensity I_{tot} and the fluorescence intensities of the PARAFAC components I_{Cn} in the two types of water and sea ice and within the specified depth ranges are listed in detail in Table 4. The median I_{tot} was the lowest in OW (I_{tot} = 0.042 R.U.) (Table 4). The components in OW in decreasing order of median fluorescence intensity were C2 > C1 > C3 > C4. There was an increase in median I_{tot} (I_{tot} = 0.056 R.U.) and a change in the composition pattern in UIW compared to OW. The components identified in UIW, in decreasing order of median fluorescence intensity I_{Cn}, were C1 > C2 > C3 > C4. The median fluorescence intensities of the EEM components I_{Cn} were significantly different in OW and UIW, as revealed by the results of the nonparametric Mann-Whitney *U* test, which measures the significance of differences between median values (Table S1). The FDOM composition, expressed as the mutual proportion of fluorescence intensities of identified components, did not change with depth in either OW or UIW. Median values of the humic-like component C2 were lower by 7.1% in surface OW compared to UIW (Fig. 4).

The decreasing order of median fluorescence intensities of the respective components I_{Cn} in the sea ice (all samples) and in the respective vertical sections of the sea ice was much the same as that in UIW (Fig. 4). The only difference between the sea ice sections was in the fluorescence intensity of the components I_{Cn} (Fig. 4c). Median I_{tot} was the lowest in the middle of the sea ice (I_{tot} = 0.029 R.U) and the highest at the bottom of the sea ice (I_{tot} = 0.0755 R.U) (Table 4). The fluorescence intensity of the protein-like component C1 was greater than the sum of fluorescence intensities of humic-like components (C2 through C4) in all considered depth section of the sea ice (Fig. 4). The median values of I_{C1} increased toward the bottom of the sea ice. The I_{C1} value recorded in the last 5 cm of the sea ice (0.083 R.U) was four times higher than in open waters.

The distribution of the median (as well as averaged) fluorescence intensities of the protein-like component C1 in the sea ice depth profiles was L-shaped, with low I_{C1} equal to ca 0.010 R.U., uniformly distributed within the upper and middle sections of the sea ice (Fig. 5). I_{C1} was more than three times greater in the last 20% of the sea ice than in the overlying sea ice layers, and reached its maximum in the last 5 cm of the sea ice (Figs. 4 and 5). The Mann-Whitney U test confirmed the statistical significance of the differences in I_{C1} values in the sea ice layers. The differences in median I_{C1} were all found to be statistically significant in the vertical sections of the sea ice except those between the surface and bottom layers (Table S1). The distribution of the median (as well as averaged) fluorescence intensities of the humic-like component C2 in the sea ice depth profiles was higher at the sea ice surface, falling to a local minimum in the middle section of the sea ice, and rising again in the bottom section (Fig. 5). The U test results confirmed that the differences in median I_{C2} in the middle sea ice section were statistically significant compared to the median I_{C2} at the surface, in the bottom sections and in the last 5 cm of the sea ice (Table S1). The distribution of the median fluorescence intensities (as well as averaged) of the other two humic-like components I_{C4} and I_{C3} in sea ice depth profiles was variable without exhibiting a clear trend (Fig. 5), and the changes in fluorescence intensity of these components were insignificant (Table S1). The fluorescence intensities of I_{C4} in the sea ice were almost one order of magnitude lower than those of I_{C1}, I_{C2} and I_{C3} (Fig. 5, Table 4).

3.4. Distribution of spectral indices in the water masses and sea ice

3.4.1. Distribution of SUVA(254) in sampled environments

The changes of DOM composition in the water masses and sea ice were confirmed by the distribution of the median (and also averaged) values of spectral indices (Table 5). The vertical distribution of spectral

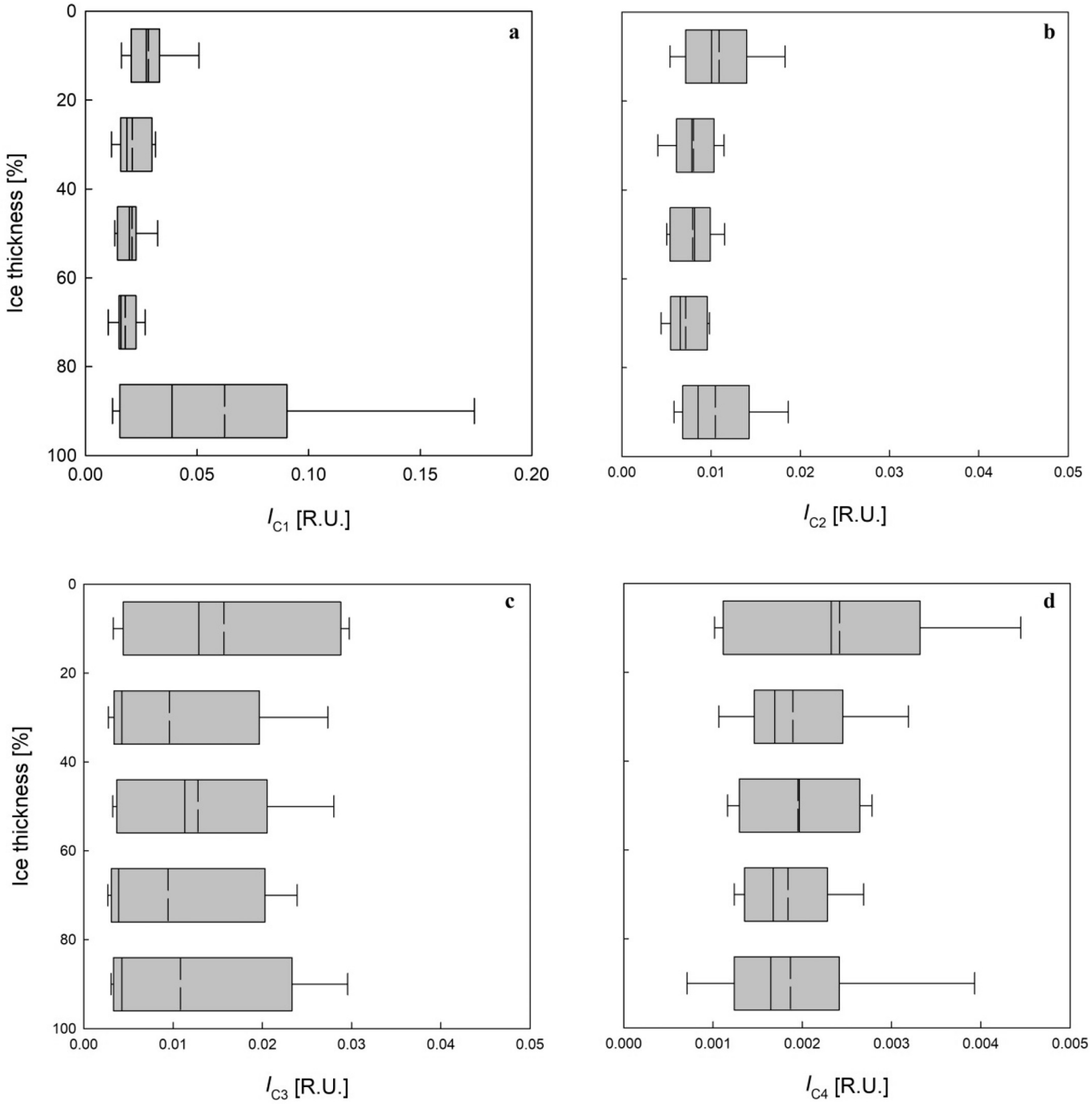

Fig. 5. Vertical profiles of fluorescence intensites of each component (a – C1, b – C2, c – C3 and d – C4) in the sea ice. The sea ice thickness is given as a percentage were 0% is the top of the sea ice and 100% is the bottom of the sea ice interacting with sea water. Averaged values are indicated by dashed lines, median values by solid lines, 10th and 90th percentiles by whiskers and 25th and 75th percentiles by boxes. Please note the change in fluorescence intensity scale between respective panels presenting statistical distribution of I_{C1}, I_{C2} and I_{C3}, and I_{C4}.).

indices within the sea ice is illustrated in Fig. 6. Low differences in CDOM absorption coefficients between OW, UIW and the sea ice (Table 2), as well as the relatively stable DOC concentration in the water bodies, resulted in a low variability of SUVA(254). Median SUVA(254) was from 3% to 15% higher in UIW than in OW (Table 5). The distribution of median SUVA(254) within the sea ice was very similar to the distribution of the median I_p/I_h ratio (Fig. 5). Median SUVA(254) in the sea ice was 6% to 32% lower than the corresponding indices recorded in OW or UIW. Median SUVA(254) increased toward the bottom of the sea ice (Table 5).

3.4.2. Distribution of HIX and I_p/I_h in sampled environments

The highest median HIX was recorded in OW with values 1.536 in below the maximum depth of chlorophyll *a* layer and 1.439 in surface OW (Table 5). The median HIXs in UIW lay between those measured in OW and ICE. Median HIX calculated for UIW was higher immediately beneath the sea ice (1.074), compared to the value of 1.046 found in the underlying maximum chlorophyll *a* depth layer (Table 5) but that difference was not statistically significant. The lowest median HIXs were measured in the sea ice: these values fell steadily from 0.629 at the surface to 0.454 in the bottom sea ice section (Fig. 6, Table 5). The

Table 5
Ranges of variability, median and 1st and 3rd quartiles (Q_1,Q_3) of the humification index (HIX), fluorescence intensity ratio of the two main groups of fluorophores (*Ip/Ih*), dissolved organic carbon concentration (DOC) and carbon specific absorption coefficient SUVA(254), in different environments. N – number of measurements.

Samples description	Statistical measure	HIX	I_p/I_h	DOC [μmol dm^{-3}]	SUVA(254) [m^2 g^{-1}C]
		Open leads water column			
Surface layer (0 - 35 m)	Min - Max	0.515–5.552	0.228–1.610	59.817–139.417	0.874–1.980
	Median	1.439	0.447	83.050	1.479
	Q_1; Q_3	1.198; 1.601	0.364; 0.491	73.392; 87.792	1.349; 1.523
	N	38	39	39	38
Below chlorophyll max. layer (35 -200 m), N = 35	Min - Max	0.738–5.217	0.203–1.095	58.325–126.917	0.879–2.093
	Median	1.563	0.387	76.108	1.449
	Q_1; Q_3	1.289; 1.887	0.342; 0.432	70.613; 84.250	1.289; 1.555
		Under ice water column			
Surface (0 m)	Min - Max	0.917–1.671	0.427–0.831	70.642–100.667	1.264–1.918
	Median	1.074	0.734	88.250	1.496
	Q_1; Q_3	0.947; 1.173	0.511; 0.7730	87.792; 92.271	1.316; 1.563
	N	8	8	6	6
Chlorophyll max. layer (3 - 25 m)	Min - Max	0.606–1.303	0.013–0.020	73.050–124.833	0.005–0.008
	Median	1.046	0.719	81.392	1.667
	Q_1; Q_3	0.951; 1.240	0.526; 0.799	73.313; 88.5	1.454; 1.704
	N	8	8	7	7
		sea ice			
Surface layer (0 - 33.3 %), N = 19	Min - Max	0.374–0.883	0.543–1.726	39.708–126.167	0.926–1.702
	Median	0.629	1.263	53.367	1.137
	Q_1; Q_3	0.478; 0.748	0.800; 1.479	44.342; 72.546	0.979; 1.369
Middle layer (33.3 - 66.6 %), N = 17	Min - Max	0.370–0.921	0.468–1.813	33.825–104.083	0.822–1.842
	Median	0.566	1.271	49.338	1.176
	Q_1; Q_3	0.509; 0.619	1.036; 1.485	42.548; 56.254	0.928; 1.338
Bottom layer (66.6 - 100 %)	Min - Max	0.127–0.893	0.597–5.303	34.467–98.583	0.657–2.245
	Median	0.454	1.361	48.250	1.390
	Q_1; Q_3	0.217; 0.715	1.026; 3.302	44.502; 68.340	1.135; 1.706
	N	21	21	14	14

median HIX recorded in the bottom sections of the sea ice was the lowest (0.454), indicating the very low saturation of DOM with humic-like substances, and was about three times less than those in OW.

The distribution of the ratio of the fluorescence intensity of the protein-like component to the sum of fluorescence intensities of humic-like components (I_p/I_h) followed the opposite trend comparing to HIX. Median I_p/I_h ratios were the lowest in OW, with the minimum of 0.387 being in the below chlorophyll max OW layer (Table 5). The contribution of protein-like fluorophores to the FDOM composition increased in UIW, resulting with 0.719 I_p/I_h median value below the sea ice and 0.734 in the maximum chlorophyll *a* depth layer (Table 5), which was nearly twice as high as in OW. I_{tot} in three separated sea ice layers was dominated by the fluorescence intensity of component C1 – I_{C1}, which was higher than the summed fluorescence intensities of the other three components. The median I_p/I_h ratios in the sea ice were > 1, and increased toward the sea ice bottom. The highest median I_p/I_h ratio in the whole data set was in the bottom section of the sea ice (1.361) (Table 5) and was more than three times as high as the averaged I_p/I_h ratio in the surface OW. The maximum I_p/I_h ratio in the bottom section of the sea ice was measured at station PS92/47 and was 5.3 in the last 5 cm section.

3.5. Enrichment factors of CDOM, FDOM and DOC in the sea ice

Compositional changes in FDOM between OW, UIW and the sea ice based solely on the absolute differences between the fluorescence intensities of the FDOM components I_{Cn}, and I_{tot} (Table 4), were statistically significant in most cases (Table S1). The significant modification of FDOM could be better expressed by calculating the enrichment factor, which takes into account the changes in intensity of a given parameter in relation to salinity. It should be noted that the results listed in Table 6 are approximate. We did not have information on the FDOM properties of the parent water, hence we followed the assumption made by Kowalczuk et al. (2017).

The enrichment factors D_c, variability range, median and 1st and 3rd quartiles (Q_1,Q_3) varied significantly for six investigated parameters (Table 6). Median values of D_c were the lowest in the surface layer of the sea ice for almost all the parameters. The median D_c calculated for component C3 was the exception, with the lowest value in the bottom layer of the sea ice. Median D_c values were the highest in the middle layer of the sea ice, with the exception of D_c calculated for the absorption coefficient $a_{CDOM}(350)$ and the protein-like component C1. For those parameters, median D_c was the highest in the bottom sea ice layers (8.0 and 16.1, respectively) (Table 6). Median D_c calculated for components C2 through C4 and the DOC concentration in the bottom section of the sea ice was lower than in the middle section. The averaged values of D_c for the last 5 cm of the sea ice were higher than those calculated for the bottom sea ice sections. The most highly enriched FDOM component was C1. The median enrichment factor for I_{C1} varied from 6.5 in the surface ice layer to 16.1 in the bottom ice layer and to 26.0 in the last 5 cm of the sea ice layer. The least enriched FDOM component was the humic-like component C4, the enrichment factor of which varied from 1.1 to 1.7. (Table 6).

The variability range of D_c was the largest (3.0–94.6) for component C1 with the highest D_c value in the middle layer of the sea ice. The

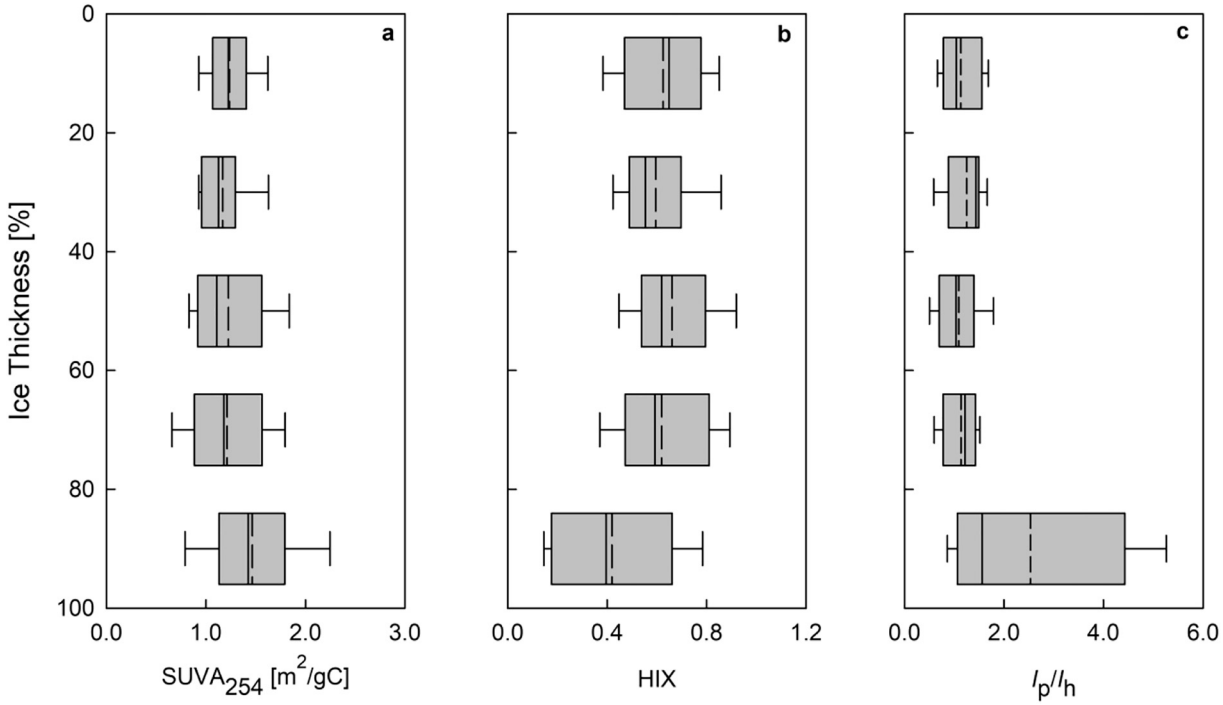

Fig. 6. Vertical profiles of: the carbon specific absoption coefficient, $SUVA_{254}$ (a), the humification index, HIX (b) and the ratio of the respective DOM fractions, I_p/I_h (c), in the sea ice. The sea ice thickness is given as a percentage were 0% is the top of the sea ice and 100% is the bottom of the sea ice interacting with sea water. Averaged values are indicated by dashed lines, median values by solid lines, 10th and 90th percentiles by whiskers and 25th and 75th percentiles by boxes.

Table 6
Ranges of variability (Min – Max), median and 1st and 3rd quartiles (Q_1, Q_3) of enrichment factors D_c for the salinity-normalized CDOM absorption coefficient at 350 nm ($a_{CDOM}(350)$), the maxima fluorescence intensity of each fluorofore ($I_{C1\text{-}C4}$), the total fluorescence intensity (I_{tot}) and dissolved organic carbon concentration, DOC, in sea ice in four subdata sets (surface, middle, bottom and last 5 cm of the sea ice layers). The calculated values of D_c for DOC in the bottom sea ice layer does not include the last 5 cm of the sea ice (missing data). The statistics do not include the D_c values calculated for station PS92/27 which were two and three orders of magnitude higher than the others and were not included to the statistic.

Sea ice layer	Statistical measure	D_c						
		$a_{CDOM(350)}$	I_{C1}	I_{C2}	I_{C3}	I_{C4}	I_{tot}	DOC
Surface layer	Min - Max	1.4–12.0	1.2–14.1	1.4–5.7	1.5–7.8	0.4–2.0	1.4–8.1	1.6–6.6
	Median	4.7	6.5	2.1	3	1.1	3.3	2.5
	Q_1; Q_3	2.1; 5.4	4.7; 7.5	1.6; 2.9	2.2; 3.9	0.7; 1.5	2.8; 4.9	2.4; 4.2
Middle layer	Min - Max	0.7–80.6	3.0–94.6	1.0–44.7	0.4–43.7	0.4–36.0	2.1–61.7	1.4–71.3
	Median	1.4	8.1	3.9	5.4	1.7	7.4	4.4
	Q_1; Q_3	0.9; 23.8	5.1; 18.4	1.8; 15.8	2.4; 26.1	0.6; 11.8	2;5; 16.3	3; 26
Bottom layer	Min - Max	3.2–13.5	3.3–43.9	1.1–8.1	1.6–11.3	0.4–2.3	2.5–19.8	1.7–11.6
	Median	8	16.1	3.4	2	1.4	7.3	3
	Q_1; Q_3	6.6; 10.7	10; 20.6	2.6; 4.6	1.8; 4.8	0.9; 2.1	5.2; 10.6	2.6; 4.2
Sea ice bottom 5 cm	Min - Max	5.4–23.3	9.5–67.1	2.3–8.8	1.7–13.1	0.6–4.8	6.7–28.0	–
	Median	13.1	26	4.6	3.5	1.1	13	–
	Q_1; Q_3	9.5; 16.2	19.4; 47.1	3.6; 6.7	2.1; 7.9	0.7; 1.6	9.5; 19.9	–

variability range of D_c was the smallest for component C4 with the lowest D_c value in the bottom layer of the sea ice (Table 6). The high variability of D_c for the FDOM components I_{tot} and DOC may be explained by the considerable heterogeneity of sea ice optical properties, the different stages of sea ice melt, and biological activity in the sea ice. At most sampling stations, we observed the beginning of sea ice melt and the start of the spring protist bloom (Kowalczuk et al., 2017; Pavlov et al., 2017), whereas winter conditions were still prevailing at the two northernmost stations PS92/43 and PS92/46 (Kowalczuk et al., 2017).

4. Discussion

4.1. Variability of FDOM, CDOM, DOC concentration and spectral indices in AW flowing into the Arctic Ocean

CDOM absorption coefficients $a_{CDOM}(350)$ in AW carried by the West Spitsbergen Current in the eastern part of the Fram Strait lay between 0.114 and 0.140 m^{-1} and were on average ca 4 times lower than those in the Polar Waters (PW) carried by the western branch of

the East Greenland Current (Granskog et al., 2012, Granskog et al., 2015a). Characteristic of the CDOM absorption in AW was its strong interannual variability (Pavlov et al., 2016; Makarewicz et al., 2018). Like $a_{CDOM}(350)$, the fluorescence intensities of the two humic-like DOM fractions representing the combined marine UV humic-like peak C and the marine humic-like peak M (Ch1 ex./em. 310/450 nm), and the UVC terrestrial humic-like peak A (Coble, 1996) (Ch2, ex./em. 280/450 nm), measured in situ in AW in the Fram Strait with a WetStar 3 – channel fluorimeter, were on average ca 4 times less than the same parameters measured in PW (Granskog et al., 2015b; Makarewicz et al., 2018). Both $a_{CDOM}(350)$ and the fluorescence intensities reported in this study closely match the published variability range of CDOM and FDOM. In spite of the strong spatial gradient of $a_{CDOM}(350)$ and fluorescence intensity across the Fram Strait, no correlation between CDOM absorption and fluorescence intensity has yet been reported in the European sector of the Arctic Ocean. We found a strong, statistically significant correlation ($R = 0.76$) between $a_{CDOM}(350)$ and I_{tot} (Fig. 7) in the sea ice. This corresponds closely with the well-established linear relationship between the CDOM absorption and DOM fluorescence intensity found in various aquatic environments (see e.g., Ferrari and Tassan, 1991; Ferrari, 2000; Kowalczuk et al., 2010).

The DOC concentration in AW varies between 40 and 170 µmol dm^{-3}, and this is likewise subject to significant interannual variability (Makarewicz et al., 2018; Engel et al., 2019). The DOC levels reported in this study lay within the variability ranges found for AW. The DOC concentrations in the sea ice were similar to the values reported by Norman et al. (2011) in Antarctic sea ice, but were on average 50% lower than those recorded by Thomas et al. (1995) in the Arctic multiyear sea ice from the Fram Strait. This observation contrasts with earlier reports on DOC concentrations in sea ice (Thomas et al., 2001; Norman et al., 2011; Stedmon et al., 2011a; Retelletti-Brogi et al., 2018): these were significantly higher than in the underlying waters in many marine basins in the Arctic and Antarctic. We found a much stronger ($R = 0.78$) and statistically significant correlation ($p < 0.001$) between the total fluorescence intensity I_{tot} and DOC concentration in the sea ice (Fig. 7). In the European section of the Arctic Ocean, a weak correlation ($R = 0.187$) between DOC and $a_{CDOM}(350)$ was reported by Makarewicz et al. (2018) in the western part of the Fram Strait.

Correlation between the total fluorescence intensity I_{tot} and DOC reported in this study influenced the variability of SUVA(254) in samples collected in OW, UIW and sea ice. The covariance of CDOM absorption and FDOM intensity with DOC concentration, together with the proportional increase in optical parameter values with increasing DOC levels, effectively reduced the variability of the absorption/DOC ratio. SUVA(254) was therefore relatively insensitive as the descriptor of compositional changes in DOM recorded in OW, UIW and sea ice. Very low values of SUVA(254) reported in this study, corresponds well to SUVA(254) variability range in the Nordic Seas (1.47–1.79), presented in the paper by Makarewicz et al. (2018). The SUVA(254) values in the European sector of Arctic Ocean were at the lower end of the global variability range of this index (Massicotte et al., 2017), what suggested an overall low saturation of CDOM with aromatic rings, the minimal influence of terrestrial DOM, and the predominantly autochthonous origin of CDOM.

Recent studies of DOM composition in sea ice, based on spectral fluorescence and multivariate statistical data analyses, reported the overall dominance of components characterized by fluorescence excitation and emission maxima in the UV, often referred to as protein-like substances, over humic-like fluorophores (Stedmon et al., 2007; Müller et al., 2011, 2013; Granskog et al., 2015b; Hill and Zimmerman, 2016; Retelletti-Brogi et al., 2018). It was also reported that the FDOM composition in sea ice differed significantly from FDOM in the surrounding sea water. Stedmon et al. (2007) found that FDOM in the waters of the Gulf of Bothnia (Baltic Sea) was dominated by humic-like components, whereas the tryptophan-like component contributed most to the FDOM intensity measured in the sea ice samples. The respective contributions of protein-like components to the total fluorescence intensity in land-fast sea ice and the underlying sea waters in the Canadian Archipelago were 95% and 79% (Hill and Zimmerman, 2016). Our observations regarding FDOM composition in the sea ice strongly support those previous findings. The percentage contribution of I_{C1} to the total fluorescence intensity varied between 17% - 62% in OW, increasing in UIW, where it varied between 30% - 62%. The proportion of I_{C1} in I_{tot} was the highest in the sea ice. The contribution of I_{C1} to I_{tot} was 35% - 63% in the surface sections of the sea ice and 32% - 64% in their middle sections. The percentage contribution of I_{C1} to the total fluorescence reached a maximum (84%) in the bottom section of the sea ice (station PS92/39), where it was attributed to the highest biomass of sympagic algae in the sea ice.

We analyzed two indices based on DOM fluorescence characteristics: the humification index HIX and the I_p/I_h ratio. Values of HIX are strongly dependent on the C/H ratio in the molecular structure of DOM, which increases with the aromaticity. High HIXs (> 10) are generally typical of freshwater environments, whereas low values (< 4) are usually found in marine waters dominated by autochthonous organic matter (Huguet et al., 2009). We measured very low HIXs in OW, lower

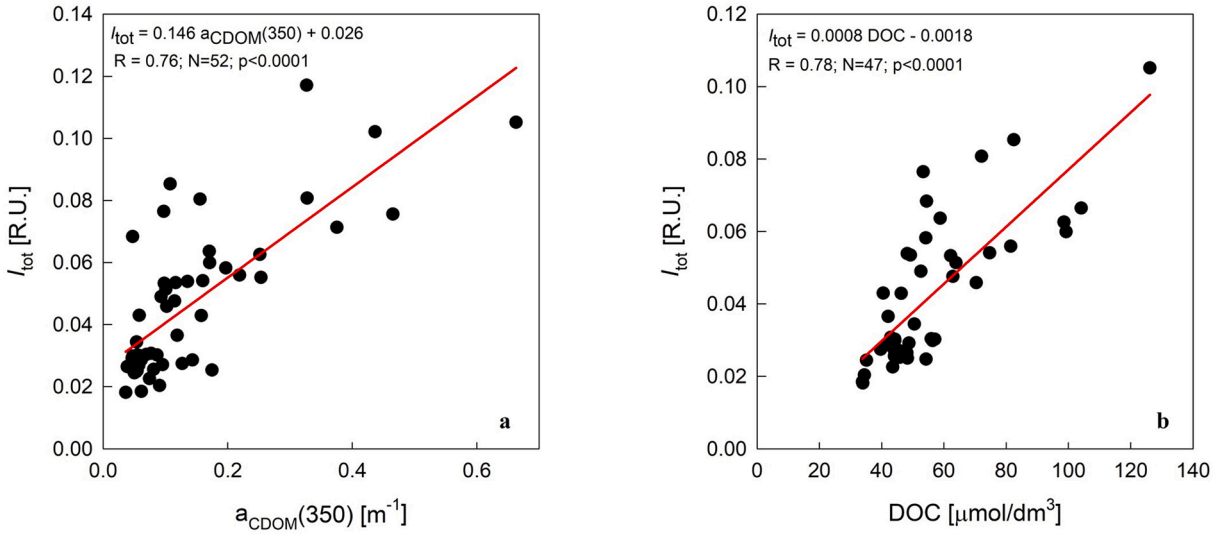

Fig. 7. Relationship between the CDOM absorption coefficient, $a_{CDOM}(350)$, and the total fluorescence intensity, I_{tot} (a), and between the concentration of dissolved organic carbon, DOC, and the total fluorescence intensity, I_{tot} (b) in the sea ice.

than those measured in the North Atlantic by Kowalczuk et al. (2013). HIX decreased in UIW and dropped below 1 in the sea ice, where it reached minimum values in the bottom ice layer (median HIX = 0.454). The minimum HIX reported here was 50% less than the minimum HIXs reported in the centers of the North and South Atlantic Subtropical Gyres (Kowalczuk et al., 2013). The I_p/I_h ratio, a measure of the proportion between protein-like and humic-like components, was the lowest in OW, but increased in UIW and sea ice, reaching a maximum in the bottom sea ice section (I_p/I_h = 1.361). The distribution of I_p/I_h clearly indicated a compositional shift of FDOM toward a higher contribution of protein-like fluorophores in the sea ice. The relative abundance of protein-like fluorophores in the sea ice was still lower than in other oceanic environments. For example, protein-like components in the surface waters of the South Atlantic Subtropical Gyre were even 15 times more abundant than humic-like fluorophores (Kowalczuk et al., 2013).

Thermal stratification of the surface layer, leading to prolonged exposure of DOM to photobleaching, was found to be the main mechanism responsible for the decrease in HIX and the increase in I_p/I_h in the subtropical gyres in the Atlantic Ocean (Kowalczuk et al., 2013). Photobleaching can hardly be regarded as an effective process leading to DOM transformation in polar waters, especially those covered by sea ice. The Arctic Ocean is dark for most of the winter, and the average spectral (305, 325, 340 and 380 nm) UV radiation doses in summer are very much lower in polar waters than in subtropical gyres (Smyth, 2011). Also, the transmittance of solar radiation through sea ice decreases significantly in the UV (Taskjelle et al., 2016); it was very low during most of this study (Massicotte et al., 2019). Therefore, other physical factors related to brine rejection during sea ice formation and biological activity within the ice should be regarded as the main processes contributing to DOM fractionation and the increase in protein-like fluorophores in the sea ice.

4.2. Enrichment factors

The median enrichment factors for the FDOM components lay within the range of previous measurements in natural sea ice (Müller et al., 2011; Granskog et al., 2015a) and artificially grown sea ice (Müller et al., 2013). They differed, however, for the major FDOM fractions, varying between 0.54 and 8.9 for protein-like fluorophores and between 0.15 and < 4 for humic-like fluorophores in the bulk sea ice samples in the different temporal stages of ice formation and persistence (Müller et al., 2011, 2013; Granskog et al., 2015a). Granskog et al. (2015a) found that the enrichment factors calculated for protein-like fluorophores increased in first-year ice in spring compared with those factors of the same class of fluorophores determined during sea ice formation, whereas D_c calculated for humic-like fluorophores remained stable. This finding leads to the conclusion that the protein-like DOM fraction accumulated in sea ice is beyond the level of initial fractionation during sea ice formation. Our observations support such a conclusion, because the enrichment factor calculated for FDOM components identified in the middle section of the sea ice, isolated from external processes that could modify the qualitative composition of FDOM, were very close to the estimates of Granskog et al. (2015a). The difference in median values of D_c calculated for the various FDOM components in the vertical sea ice sections may be the consequence of physical and biological processes leading to further FDOM fractionation other than brine rejection during sea ice formation. The lower median D_c values recorded in the upper sections of the sea ice, near the ice surface (Table 6), could be an indication of the relative weathering and mineralization of DOM (D_c lower for DOC), presumably by photodegradation, even at low solar irradiance intensities of UV (Smyth, 2011). Median D_c obtained for $a_{CDOM}(350)$ and I_{C1} in the bottom sea ice were higher than in the middle section but those calculated for I_{C2}, I_{C3} and I_{C4} were lower. This could be an indication of the removal of humic-like FDOM components along with brine rejection. Sea ice porosity and brine content were higher at the bottom of the sea ice than in the overlying layers. The temperature and salinity at the bottom of the sea ice were both higher than in the overlying layers (Table 2), which suggests that melting and brine channel opening may be starting, enabling the gravitational leakage of brines into the underlying UIW. The higher D_c values for $a_{CDOM}(350)$ and I_{C1} suggest the accumulation of CDOM and protein-like FDOM as a result of sympagic algae production. In the last 5 cm of the sea ice, close to the UIW interface, median D_c was higher with respect to all the parameters considered except I_{C4}. This suggests that biological production, which is at its most intensive at the bottom of the sea ice, is capable of compensating for the loss of some humic-like components due to following removal with the brine.

Owing to the heterogeneity of the optical properties of sea ice and the uneven distribution of autotrophic organisms in the sea ice, coupling between the biological production of DOM and its optical properties (CDOM absorption, FDOM intensity) has been postulated on the basis of a qualitative comparison of the mutual positions of the maxima of optical and bio-optical parameters in the vertical cross section of the sea ice. The maxima of CDOM absorption, FDOM intensities and chlorophyll *a* concentration were recorded in the bottom section of the sea ice (Xie et al. (2014), Hill and Zimmerman (2016), Kowalczuk et al. (2017), the current study). For example, the shape of the vertical distribution of I_{C1} is very similar to that of the median chlorophyll *a* concentration *Tchla* in the sea ice (Kowalczuk et al., 2017). The vertical distribution of median I_{C2} in the sea ice (Fig. 5) is very similar to that of $a_{CDOM}(350)$ within the sea ice (Fig. 2). Observations of the seasonal dynamics of the chlorophyll *a* concentration and CDOM absorption also suggest strong coupling and temporal coordination between an increase in magnitude of optical parameters and an increase in *Tchla* in the sea ice and UIW (Xie et al., 2014; Kowalczuk et al., 2017; Pavlov et al., 2017). We performed a regression analysis between $a_{CDOM}(350)$, $I_{C1\text{-}C4}$, I_{tot} and *Tchla* to find evidence in support of the hypothesis postulating the significant production of CDOM/FDOM by sympagic algae communities. We found a relatively strong (R = 0.63) and statistically significant (p < 0.0001) correlation between I_{C1} and *Tchla* in the log-log scale (Fig. 8). This is the first quantitative evidence documenting coupling between the sympagic algae biomass and protein-like FDOM in Arctic Ocean sea ice. Xie et al. (2014) observed a significant correlation between chlorophyll *a* concentration and $a_{CDOM}(325)$ in first-year and land-fast sea ice in the western Canadian Arctic. The direct production of a protein-like FDOM component by autotrophic protist communities was discovered in polar waters by Yamashita et al. (2017) in the Polar North Pacific and by Makarewicz et al. (2018) in the Nordic Seas. Therefore, the exceptionally high enrichment factors calculated for I_{C1} in the last 5 cm of the sea ice should be considered as an effect of biological production. Marine bacterial communities are capable of efficiently producing both protein-like and humic-like FDOM fractions growing on phytoplankton exudates (Romera-Castillo et al., 2010, 2011).

Biological production, and presumably the microbial transformation of fresh DOM in the ice, cannot compensate for the general decrease in optical DOM characteristics in Arctic Ocean surface water during the summer sea ice melt. The photodegradation of autochthonous DOM produced in the ice might explain the existence of short-lived DOM in the Arctic Ocean surface layer as a result of sea ice melt. Xie et al. (2014) and Hill and Zimmerman (2016) found that autochthonous DOM produced by sympagic algae was highly photoreactive and was quickly removed, even at the low UV radiation intensities in the Arctic. Although autochthonous DOM consists mostly of LWM nitrogen-rich, bioavailable organic compounds, these should not be considered as a potential source of organic nutrients. Observations in the Arctic Ocean in late summer showed that the surface water influenced by melt water is highly transparent, with low levels of CDOM and particulate absorption and chlorophyll *a* fluorescence (Ardyna et al., 2011; Granskog et al., 2015b; Kowalczuk et al., 2019).

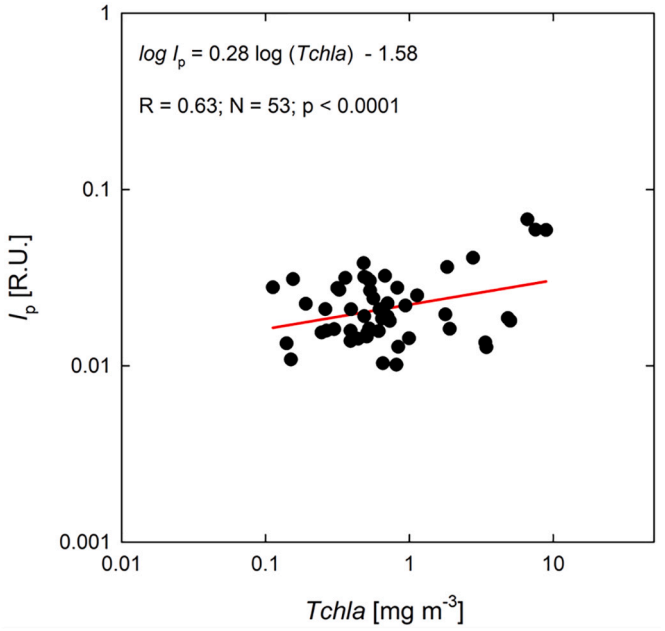

Fig. 8. Relationship between the concentration of total chlorophyll, *Tchla*, and the fluorescence intensity of the protein-like component (I_p) identified by PARAFAC in the sea ice.

5. Conclusions

Ice and water column samples collected during the TRANSSIZ expedition on board the FS Polarstern (cruise code PS92 - ARK XXIX/1) in May and June 2015 to the Sophia Basin and Yermak Plateau, north of the Svalbard Archipelago, enabled us to characterize FDOM properties in open waters (OW), under-ice waters (UIW) and sea ice. By applying multivariate statistical modelling (PARAFAC) to DOM fluorescence excitation-emission matrices, we identified four FDOM components. Based on the spectral signatures of these components, we classified component C1 as a protein-like FDOM fraction having spectral characteristics similar to tryptophan. The three other components (C2 through C4) were classified as humic-like components with spectral characteristics similar to marine LMW humic substances and terrestrial humic-like substances. We found a significant shift in FDOM composition toward the increasing prevalence of protein-like components in UIW and sea ice in comparison to OW. The FDOM composition in oceanic OW was dominated by humic-like components. In the sea ice, the fluorescence intensity of C1 was ca 1.3 times higher than the sum of C2 through C4. On the basis of the calculated spectral indices, we also found a significant shift of FDOM toward higher amounts of LMW organic compounds, which agrees very well with the findings of Müller et al. (2011) and Retelletti-Brogi et al. (2018).

The absolute DOC concentration and the optical DOM characteristics, i.e. $a_{CDOM}(350)$, and the fluorescence intensities of components $I_{C2\text{-}C4}$ were lower in the sea ice than in OW and UIW. The salinity-normalized components revealed significant enrichments of the various DOM optical characteristics in the sea ice. The fluorescence intensity of the protein-like component C1 I_{C1} was enriched the most – up to 26 times, whereas that of the terrestrial humic-like component C4 I_{C4} was enriched the least – 1.1 to 1.7 times relative to the salinity.

The modification of the FDOM composition in the sea ice was an effect of multiple processes: the fractionation of DOM during ice formation, as described by Müller et al. (2011, 2013), the transformation of DOM retained in the ice crystal structures and brine canals over the winter, and the production of DOM by sympagic algae (e.g., Xie et al., 2014; Retelletti-Brogi et al., 2018) in spring and its possible photodegradation in the surface ice layer by the solar radiation incident on the ice surface following snow melt. Based on the statistically significant correlation between I_{C1} and *Tchla*, we demonstrated that the biological production of protein-like fluorophores by sympagic algal communities is a major process leading to the very high accumulation of LWM, nitrogen-rich organic compounds in the sea ice in the European section of the Arctic Ocean.

Supplementary data to this article can be found online at https://doi.org/10.1016/j.marchem.2020.103893.

Declaration of Competing Interest

None.

Acknowledgements

This work was supported by the Polish-Norwegian Research Program operated by the National Centre for Research and Development under the Norwegian Financial Mechanism 2009–2014 within the framework of Project Contract Pol-Nor/197511/40/2013, CDOM-HEAT, awarded to PK. The TRANSSIZ cruise (Transitions in the Arctic Seasonal Sea Ice Zone; ARKXXIX/1-PS92; grant AWI_PS92_00) was initiated and co-organized by the Arctic in Rapid Transition (ART) network, and parts of this study were funded by the Polar Biological Oceanography Group of the Alfred Wegener Institute, Helmholtz Centre for Polar and Marine Research within PACES II. TRANSSIZ data are available from the corresponding author.

References

Aagaard, K., Foldvik, A., Hillman, S.R., 1987. The West Spitsbergen Current: Disposition and water mass transformation. J. Geophys. Res. 92 (C4). https://doi.org/10.1029/JC092iC04p03778. 3778–3784.

Ardyna, M., Gosselin, M., Michel, C., Poulin, M., Tremblay, J.-É., 2011. Environmental forcing of phytoplankton community structure and function in the Canadian High Arctic: contrasting oligotrophic and eutrophic regions. Mar. Ecol. Prog. Ser. 442, 37–57.

Arrigo, K., 2017. Sea ice as a habitat for primary producers. In: Thomas, D.N. (Ed.), Sea Ice. John Wiley & Sons, Ltd, Chichester 362–269.

Barlow, L.K., Rogers, J.C., Serreze, M.C., Barry, R.G., 1997. Aspects of climate variability in the North Atlantic sector: discussion and relation to the Greenland ice sheet project 2 high-resolution isotopic signal. J. Geophys. Res. 102https://doi.org/10.1029/96JC02401. (issn: 0148-0227).

Beszczynska-Möller, A., Fahrbach, E., Schauer, U., Hansen, E., 2012. Variability in Atlantic water temperature and transport at the entrance to the Arctic Ocean, 1997–2010. ICES J. Mar. Sci. 69 (5), 852–863. https://doi.org/10.1093/icesjms/fss056.

Catalá, T.S., Álvarez-Salgado, X.A., Otero, J., Iuculano, F., Companys, B., Horstkotte, B., et al., 2016. Drivers of fluorescent dissolved organic matter in the global epipelagic ocean. Limnol. Oceanogr. 61 (3), 1101–1119.

Coble, P.G., 1996. Characterization of marine and terrestrial DOM in seawater using-excitation–emission matrix spectroscopy. Mar. Chem. 51, 325–346.

Dainard, P.G., Guéguen, C., 2013. Distribution of PARAFAC modeled CDOM components in the North Pacific Ocean, Bering, Chukchi and Beaufort seas. Mar. Chem. 157, 216–223.

Ehn, J., Granskog, M.A., Reinart, A., Erm, A., 2004. Optical properties of melting landfast sea ice and underlying sea water in Santala Bay, Gulf of Finland. J. Geophys. Res.–Oceans 109, C09003. https://doi.org/10.1029/2003JC002042.

Engel, A., Bracher, A., Dinter, T., Endres, S., Grosse, J., Metfies, K., Peeken, I., Piontek, J., Salter, I., Nöthig, E.-M., 2019. Inter-annual variability of organic carbon concentration in the eastern Fram Strait during summer (2009 – 2017). Front. Mar. Sci. 6, 187. https://doi.org/10.3389/fmars.2019.00187.

Ferrari, G., 2000. The relationship between chromophoric dissolved organic matter and dissolved organic carbon in the European Atlantic coastal area and in the West Mediterranean Sea (Gulf of Lions). Mar. Chem. 70 (4), 339–357.

Ferrari, G., Dowell, M., 1998. CDOM absorption characteristics with relation to fluorescence and salinity in coastal areas of the southern Baltic Sea. Estuar. Coast. Shelf S. 47 (1) 91–10.

Ferrari, G., Tassan, S., 1991. On the accuracy of determining light absorption by "yellow substance"through measurement of induced fluorescence. Limnol. Oceanogr. 36 (4), 777–786.

Gonçalves-Araujo, R., Stedmon, C.A., Heim, B., Dubinenkov, I., Kraberg, A., Moiseev, D., Bracher, A., 2015. From fresh to marine waters: characterization and fate of dissolved organic matter in the Lena River delta region, Siberia. Front. Mar. Sci. 2, 108. https://doi.org/10.3389/fmars.2015.00108.

Gonçalves-Araujo, R., Granskog, M., Bracher, A., Zetsu-Scott, K., Dott, P.A., Stedmon, C.A., 2016. Using fluorescent dissolved organic matter to trace and distinguish the

origin of Arctic surface waters. Sci. Rep. 6, 33978. https://doi.org/10.1038/srep33978.
Gonçalves-Araujo, R., Rabe, B., Peeken, I., Bracher, A., 2018. High colored dissolved organic matter (CDOM) absorption in surface waters of the Central-Eastern Arctic Ocean: implications for biogeochemistry and ocean color algorithms. PLoS One 13 (1), e0190838. https://doi.org/10.1371/journal.pone.0190838.
Granskog, M.A., Stedmon, C.A., Dodd, P.A., Amon, R.M.W., Pavlov, A.K., de Steur L.and Hansen E., 2012. Characteristics of colored dissolved organic matter (CDOM) in the Arctic outflow in the Fram Strait: Assessing the changes and fate of terrigenous CDOM in the Arctic Ocean. J. Geophys. Res.-Oceans 177 (12). https://doi.org/10.1029/2012JC008075.
Granskog, M.A., Nomura, D., Müller, S., Krell, A., Toyota, T., Hattori, H., 2015a. Evidence for significant protein-like dissolved organic matter accumulation in Sea of Okhotsk sea ice. Ann. Glaciol. 56 (69). https://doi.org/10.3189/2015AoG69A002. 8 pp.
Granskog, M.A., Pavlov, A.K., Sagan, S., Kowalczuk, P., Raczkowska, A., Stedmon, C.A., 2015b. Effect of sea-ice melt on inherent optical properties and vertical distribution of solar radiant heating in Arctic surface waters. J. Geophys. Res.-Oceans 120, 7028–7039. https://doi.org/10.1002/2015JC011087.
Granskog, M.A., Rösel, A., Dodd, P.A., Divine, D., Gerland, S., Martma, T., Leng, M.J., 2017. Snow contribution to first-year and second-year Arctic Sea ice mass balance north of Svalbard. J. Geophys. Res.-Oceans 122, 2539–2549. https://doi.org/10.1002/2016JC012398.
Grenfell, T.C., Perovich, D.K., 1981. Radiation absorption coefficients of polycrystalline ice from 400–1400 nm. J. Geophys. Res.-Oceans 86 (C8), 7447–7450.
Guéguen, C., Cuss, C.W., Cassels, C.J., Carmack, E.C., 2014. Absorption and fluorescence of dissolved organic matter in the waters of the Canadian Arctic archipelago, Baffin Bay, and the Labrador Sea. J. Geophys. Res.-Oceans 119, 2034–2047. https://doi.org/10.1002/2013JC009173.
Guéguen, C., Itoh, M., Kikuchi, T., Eert, J., Williams, W.J., 2015. Variability in dissolved organic matter optical properties in surface waters in the Amerasian Basin. Front. Mar. Sci. 2, 78. https://doi.org/10.3389/fmars.2015.00078.
Hansen, E., Gerland, S., Granskog, M.A., Pavlova, O., Renner, A.H.H., Haapala, J., Løyning, T.B., Tschudi, M., 2013. Thinning of Arctic Sea ice observed in Fram Strait: 1990–2011. J. Geophys. Res.-Oceans 118, 5202–5221. https://doi.org/10.1002/jgrc.20393.
Harshman, R.A., 1984. How can I know if it's 'real'? A catalog of diagnostics for use with three-mode factor analysis and multidimensional scaling. In: Law, H.G., Snyder Jr.C.W., Hattie, J.A., McDonald, R. (Eds.), Research Methods for Multimode Data Analysis. Praeger, New York, pp. 566–591.
Hill, V., Zimmerman, R., 2016. Characteristic of colored dissolved organic material in first year landfast sea ice and the underlying water column in the Canadian Arctic in the early spring. Mar. Chem. 180, 1–13.
Huguet, A., Vacher, L., Relexans, S., Saubusse, S., Froidefond, J.M., Parlanti, E., 2009. Properties of fluorescent dissolved organic matter in the Gironde estuary. Org. Geochem. 40 (6), 706–719.
Jerlov, N.G., 1976. Marine Optics. Elsevier, New York 231 pp.
Jørgensen, L., Stedmon, C.A., Kragh, T., Markager, S., Middelboe, M., Søndergaard, M., 2011. Global trends in the fluorescence characteristics and distribution of marine dissolved organic matter. Mar. Chem. 126, 139–148.
Kalle, K., 1938. Zum Probleme der Meereswasserfarbe. Ann. Hydrol. Mar. Mitt. 66, 1–13.
Katlein, C., Arndt, C.S., Belter, H.J., Castellani, G., Nicolaus, M., 2019. Seasonal evolution of light transmission distributions through Arctic sea ice. J. Geophys. Res.- Oceans, 124, 5418–5435. https://doi.org/10.1029/2018JC014833.
Kauko, H.M., Taskjelle, T., Assmy, P., Pavlov, A.K., Mundy, C.J., Duarte, P., 2017. Windows in Arctic Sea ice: Light transmission and ice algal optical properties in a refrozen lead. J. Geophys. Res.–Biogeo. 122, 1486–1505. https://doi.org/10.1002/2016JG003626.
Kothawala, D.N., Stedmon, C.A., Müller, R.A., Weyhenmeyer, G.A., Köhler, S.J., Tranvik, L.J., 2014. Controls of dissolved organic matter quality: evidence from a large-scale boreal lake survey. Glob. Chang. Biol. 20, 1101–1114. https://doi.org/10.1111/gcb.12488.
Kowalczuk, P., Stedmon, C.A., Markager, S., 2006. Modelling absorption by CDOM in the Baltic Sea from season, salinity and chlorophyll. Mar. Chem. 101, 1–11.
Kowalczuk, P., Durako, M.J., Young, H., Kahn, A.E., Cooper, W.J., Gonsior, M., 2009. Characterization of dissolved organic matter fluorescence in the South Atlantic bight with use of PARAFAC model: interannual variability. Mar. Chem. 113, 182–196.
Kowalczuk, P., Zabłocka, M., Sagan, S., Kuliński, K., 2010. Fluorescence measured in situ as a proxy of CDOM absorption and DOC concentration in the Baltic Sea. Oceanologia 52 (3), 431–471.
Kowalczuk, P., Tilstone, G.H., Zabłocka, M., Röttgers, R., Thomas, R., 2013. Composition of dissolved organic matter along an Atlantic meridional transect from fluorescence spectroscopy and parallel factor analysis. Mar. Chem. 157, 170–184.
Kowalczuk, P., Meler, J., Kauko, H., Pavlov, A.K., Zabłocka, M., Peeken, I., 2017. Bio–optical properties of Arctic drif ice and surface waters north of Svalbard from winter to spring. J. Geophys. Res.– Oceans 122 (6) 4634–466.
Kowalczuk, P., Sagan, S., Makarewicz, A., Meler, J., Borzycka, K., Zabłocka, M., 2019. Bio-optical properties of surface waters in the Atlantic water inflow region off Spitsbergen (Arctic Ocean). J. Geophys. Res.– Oceans 124https://doi.org/10.1029/2018JC014529. 1964–1987.
Light, B., Perovich, D.K., Webster, M.A., Polashenski, C., Dadic, R., 2015. Optical properties of melting first-year Arctic sea ice. J. Geophys. Res.– Oceans 120, 7657–7675. https://doi.org/10.1002/2015JC011163.
Logvinova, C.L., Frey, K.E., Cooper, L.W., 2016. The potential role of sea ice melt in the distribution of chromophoric dissolved organic matter in the Chukchi and Beaufort seas. Deep-Sea Res. 130 (Part II), 28–42.
Makarewicz, A., Kowalczuk, P., Sagan, S., Granskog, M.A., Pavlov, A.K., Zdun, A., 2018. Characteristics of chromophoric and fluorescent dissolved organic matter in the Nordic seas. Ocean Sci. 14, 543–562.
Massicotte, P., Asmala, E., Stedmon, C.A., Markager, S., 2017. Global distribution of dissolved organic matter along the aquatic continuum: across rivers, lakes and oceans. Sci. Total Environ. 609, 180–191. https://doi.org/10.1016/j.scitotenv.2017.07.076.
Massicotte, P., Peeken, I., Katlein, C., Flores, H., Huot, Y., Castellani, G., Arndt, S., Lange, B.A., Tremblay, J.E., Babin, M., 2019. Sensitivity of phytoplankton primary production estimates to available irradiance under heterogeneous sea ice conditions. J. Geophys. Res. – Oceans 124 5436-5450.
McPhee, M.G., 2017. The sea ice–ocean boundary layer. In: Thomas, D.N. (Ed.), Sea Ice. John Wiley & Sons, pp. 138–159. https://doi.org/10.1002/9781118778371.ch5.
Meyer, A., Sundfjord, A., Fer, I., Provost, Ch., Robineau, N.V., Koenig, Z., 2017. Winter to summer oceanographic observations in the Arctic Ocean north of Svalbard. J. Geophys. Res.-Oceans 122, 6218–6237pp. https://doi.org/10.1002/2016JC012391.
Miller, L.A., Fripiat, F., Else, B.G., Bowman, J.S., Brown, K.A., Collins, R.E., 2015. Methods for biogeochemical studies of sea ice: the state of the art, caveats, and recommendations. Elementa: Sci. Anthrop. 3 (000038), 1–53. https://doi.org/10.12952/journal.elementa.000038.
Müller, S., Vähätalo, A.V., Granskog, M.A., Autio, R., Kaartokallio, H., 2011. Behaviour of dissolved organic matter during formation of natural and artificially grown Baltic Sea ice. Ann. Glaciol. 52 (57), 233–241.
Müller, S., Vähätalo, A.V., Stedmon, C.A., Granskog, M.A., Norman, L., Aslam, S.N., 2013. Selective incorporation of dissolved organic matter (DOM) during sea ice formation. Mar. Chem. 155, 148–157.
Murphy, K.R., Butler, K.D., Spencer, R.G.M., Stedmon, C.A., Boehme, J.R., Aiken, G.R., 2010. Measurement of dissolved organic matter fluorescence in aquatic environments: an Interlaboratory comparison. Environ.Sci. Technol. 44 (24), 9405–9412. https://doi.org/10.1021/es102362t.
Murphy, K.R., Stedmon, C.A., Graeber, D., Bro, R., 2013. Fluorescence spectroscopy and multi–way techniques. PARAFAC, Anal. Methods-UK 5, 6557. https://doi.org/10.1039/c3ay41160e.
Murphy, K.R., Stedmon, C.A., Wenig, P., Bro, R., 2014. OpenFluor – an online spectral library of auto–fluorescence by organic compounds in the environment, anal. Methods-UK 6, 658–661. https://doi.org/10.1039/C3AY41935E.
Norman, L., Thomas, D.N., Stedmon, C.A., Granskog, M.A., Papadimitriou, S., Krapp, R.H., et al., 2011. The characteristics of dissolved organic matter (DOM) and chromophoric dissolved organic matter (CDOM) in Antarctic Sea ice. Deep-Sea Res. II 58, 1075–1091.
Onarheim, I.H., Smedsrud, L.H., Ingvaldsen, R.B., Nilsen, F., 2014. Loss of sea ice during winter north of Svalbard. Tellus A 66 (1), 23933. https://doi.org/10.3402/tellusa.v66.23933.
Pavlov, A.K., Granskog, M.A., Stedmon, C.A., Ivanov, B.V., Hudson, S.R., Falk-Petersen, S., 2015. Contrasting optical properties of surface waters across the Fram Strait and its potential biological implications. J. Mar. Syst. 143, 62–72.
Pavlov, A.K., Stedmon, C.A., Semushin, A.V., Martma, T., Ivanov, B.V., Kowalczuk, P., Granskog, M.A., 2016. Linkages between the circulation and distribution of dissolved organic matter in the White Sea. Arctic Ocean. Cont. Shelf Res. 119, 1–13. https://doi.org/10.1016/j.csr.2016.03.004.
Pavlov, A.K., Taskjelle, T., Kauko, H.M., Hamre, B., Hudson, S.R., Assmy, P., 2017. Altered inherent optical properties and estimates of the underwater light field during an Arctic under ice bloom of Phaeocystispouchetii. J. Geophys. Res.–Oceans 122, 4939–4961. https://doi.org/10.1002/2016JC012471.
Peeken, I., 2016. The Expedition PS92 of the Research Vessel POLARSTERN to the Arctic Ocean in 2015, Berichte zur Polar- und Meeresforschung Reports on polar and marine research, Bremerhaven, Alfred Wegener Institute for Polar and Marine Research. pp. 694. 153 p. https://doi.org/10.2312/BzPM_0694_2016.
Perovich, D.K., 2017. Sea ice and sunlight, in: sea ice, 2017. Thomas, D.N. (Eds.) 3rd ed. Wiley, Chichester, Chapter 4. pp. 110–137.
Perovich, D.K., Govoni, J.W., 1991. Absorption coefficients of ice from 250 to 400 nm. Geophys. Res. Lett. 18 (7), 1233–1235.
Perovich, D.K., Cota, G.F., Maykut, G.A., Grengfell, T.C., 1993. Bio-optical observations of first-year Arctic Sea ice. Geophys. Res. Lett. 20 (11), 1059–1062.
Polyakov, I.V., Pnyushkov, A.V., Alkire, M.B., Ashik, I.M., Baumann, T.M., Carmack, E.C., 2017. Greater role for Atlantic inflows on sea-ice loss in the Eurasian Basin of the Arctic Ocean. Science 356, 285–291. https://doi.org/10.1126/science.aai8204.
Renner, A.H.H., Gerland, S., Haas, C., Spreen, G., Beckers, J.F., Hansen, E., 2014. Evidence of Arctic Sea ice thinning from direct observations. Geophys. Res. Lett. 41 (14), 5029–5036. https://doi.org/10.1002/2014gl060369.
Retelletti-Brogi, S., Ha, S.Y., Kim, K., Derrien, M., Lee, Y.K., Hur, J., 2018. Optical and molecular characterization of dissolved organic matter(DOM) in the Arctic ice core and the underlying seawater (Cambridge Bay, Canada): implication for increased autochthonous DOM during ice melting. Sci. Total Environ. 627, 802–811.
Romera-Castillo, C., Sarmento, H., Álvarez-Salgado, X.A., Gasol, J.M., Marrasé, C., 2010. Production of chromophoric dissolved organic matter by marine phytoplankton. Limnol. Oceanogr. 55 (1), 446–454.
Romera-Castillo, C., Sarmento, H., Álvarez-Salgado, X.A., Gasol, J.M., Marrasé, C., 2011. Net production and consumption of fluorescent colored dissolved organic matter by natural bacterial assemblages growing on marine phytoplankton exudates. Appl. Environ. Microbiol. 7490–7498.
Sharp, J.M., 2002. Analytical methods for total DOM pools. In: Hansell, D.A., Carlson, C.A. (Eds.), Biogeochemistry of Marine Dissolved Organic Matter. Elsevier Science, San Diego, pp. 35–58.
Smyth, T.J., 2011. Penetration of UV irradiance into the global ocean. J. Geophys. Res.-Oceans 116https://doi.org/10.1029/2011JC007183. C11020.
Søndergaard, M., Borch, N.H., Stedmon, C.A., 2003. Fate of terrigenous dissolved organic

matter (DOM) in estuaries: aggregation and bioavailability. Ophelia 57, 161–176. https://doi.org/10.1080/00785236.2003.10409512.
Stedmon, C.A., Bro, R., 2008. Characterizing dissolved organic matter fluorescence with parallel factor analysis: a tutorial. Limnol. Oceanogr. Methods 6. https://doi.org/10.4319/lom.2008.6.572.
Stedmon, C.A., Markager, S., 2001. The optics of chromophoric dissolved organic matter (CDOM) in the Greenland Sea: an algorithm for differentiation between marine and terrestrially derived organic matter, Limnol. Oceanogr. 46 (8) 2087–2.
Stedmon, C.A., Markager, S., 2005a. Resolving the variability in dissolved organic matter fluorescence in a temperate estuary and its catchment using PARAFAC analysis. Limnol. Oceanogr. 50 (5), 686–697.
Stedmon, C.A., Markager, S., 2005b. Tracing the production and degradation of autochthonous fractions of dissolved organic matter by fluorescence analysis. Limnol. Oceanogr. 50 (5), 1415–1426.
Stedmon, C.A., Markager, S., Kaas, H., 2000. Optical properties and signatures of chromophoric dissolved organic matter (CDOM) in Danish coastal waters. Estuar. Coast. Shelf S. 51, 267–278.
Stedmon, C.A., Markager, S., Bro, R., 2003. Tracing dissolved organic matter in aquatic environments using a new approach to fluorescence spectroscopy. Mar. Chem. 82 (3–4), 239–254. https://doi.org/10.1016/S0304-4203(03)00072-0.
Stedmon, C.A., Thomas, D.N., Granskog, M.A., Kaartokallio, H., Papadimitriou, S., Kuosa, H., 2007. Characteristics of dissolved organic matter in Baltic coastal sea ice: Allochthonous or autochthonous origins? Environ. Sci. Technol. 41 (21), 7273–7279.
Stedmon, C.A., Amon, R.M.W., Rinehart, A.J., Walker, S.A., 2011a. The supply and characteristics of colored dissolved organic matter (CDOM) in the Arctic Ocean: Pan Arctic trends and differences. Mar. Chem. 124, 108–118.
Stedmon, C.A., Thomas, D.N., Papadimitriou, S., Granskog, M.A., Dieckmann, G.S., 2011b. Using fluorescence to characterize dissolved organic matter in Antarctic sea ice brines. J. Geophys. Res.-Biogeosci. 116, 1–9 2011JG001716.
Taskjelle, T., Hudson, S.R., Granskog, M.A., Nicolaus, M., Lei, R., Gerland, S., et al., 2016. Spectral albedo and transmittance of thin young Arctic sea ice. J. Geophys. Res.–Oceans 121https://doi.org/10.1002/2015JC011254. 540–553.
Taskjelle, T., Granskog, M.A., Pavlov, A.K., Hudson, S.R., Hamre, B., 2017. Effects of an Arctic under-ice bloom on solar radiant heatingof the water column. J. Geophys. Res.–Oceans 122, 126–138. https://doi.org/10.1002/2016JC012187.
Thomas, D.N. (Ed.), 2017. Sea ice, 3rd edn. Wiley-Blackwell, West Sussex.
Thomas, D.N., Lara, R.J., Eicken, H., Kattner, G., Skoog, A., 1995. Dissolved organic matter in Arctic multi-year sea ice during winter: major components and relationship to ice characteristics. Polar Biol. 15, 477–483. https://doi.org/10.1007/BF00237461.
Thomas, D.N., Kattner, G., Engbrodt, R., Giannelli, V., Haas, C., Dieckmann, G.S., 2001. Dissolved organic matter in Antarctic Sea ice. Ann. Glaciol. 33, 297–303.
Uusikivi, J., Vähätalo, A.V., Granskog, M.A., Sommaruga, R., 2010. Contribution of mycosporine-like amino acids and colored dissolved and particulate matter to sea ice optical properties and ultraviolet attenuation, Limnol. Oceanogr. 55 (2), 703–713.
Vodacek, A., Blough, N.V., DeGrandpre, M.D., Peltzer, E.T., Nelson, R.K., 1997. Seasonal variation of CDOM and DOC in the middle Atlantic bight: terrestrial inputs and photooxidation. Limnol. Oceanogr. 42 (2), 674–686.
Weishaar, J.L., Aiken, G.R., Bergamaschi, B.A., Fram, M.S., Fujii, R., Mopper, K., 2003. Evaluation of specific ultraviolet absorbance as an Indicator of the chemical composition and reactivity of dissolved organic carbon. Environ. Sci. Technol. 37 (20), 4702–4708. https://doi.org/10.1021/es030360x.
Woźniak, B., Dera, J., 2007. Light Absorption in Sea Water. In: 456 pp. Springer, New York.
Xie, H., Aubry, C., Zhang, Y., Song, G., 2014. Chromophoric dissolved organic matter (CDOM) in first-year sea ice in western Canadian Arctic. Mar. Chem. 165, 25–35.
Yamashita, Y., Hashihama, F., Saito, H., Fukuda, H., Ogawa, H., 2017. Factors controlling the geographical distribution of fluorescent dissolved organic matter in the surface waters of the Pacific Ocean. Limnol. Oceanogr. 62, 2360–2374. https://doi.org/10.1002/lno.10570.
Zsolnay, A., Baigar, E., Jimenez, M., Steinweg, B., Saccomandi, F., 1999. Differentiating with fluorescence spectroscopy the sources of dissolved organic matter in soils subjected to drying. Chemosphere 38 (1), 45–50. https://doi.org/10.1016/S0045-6535(98)00166-0.